NACA TN 2232

NATIONAL ADVISORY COMMITTEE FOR AERONAUTICS

TECHNICAL NOTE 2232

STRESS AND DISTORTION ANALYSIS OF A SWEPT BOX BEAM HAVING BULKHEADS PERPENDICULAR TO THE SPARS

By Richard R. Heldenfels, George W. Zender, and Charles Libove

Langley Aeronautical Laboratory
Langley Air Force Base, Va.

Washington

November 1950

NATIONAL ADVISORY COMMITTEE FOR AERONAUTICS

TECHNICAL NOTE 2232

STRESS AND DISTORTION ANALYSIS OF A SWEPT BOX BEAM HAVING BULKHEADS PERPENDICULAR TO THE SPARS

By Richard R. Heldenfels, George W. Zender, and Charles Libove

SUMMARY

A method is presented for the approximate calculation of the stresses and distortions in a box beam representing the main structural component of a swept wing with a carry-through section and with bulkheads perpendicular to the spars. The outer and carry-through sections of such a wing can be analyzed by existing methods if some means is provided for analyzing the triangular section which connects them. In the method presented the triangular section is divided into free bodies and then equilibrium and continuity are established between these bodies. The result is a system of linear equations which can be solved for the rotations and translations of the three vertical edges of the triangular section.

The application of the method is illustrated by a numerical example and the results are compared with previously published test data. The agreement is fair, with the principal discrepancies being due to the fact that the method is based on a very simple type of idealized structure which prevents the appearance of shear lag in the results. Extension of the basic approach to permit the inclusion of shear lag is indicated. The effects of the shear and bending flexibility of the bulkheads bordering the triangular section are investigated and are shown to be important.

INTRODUCTION

Experimental investigations of swept box beams (references 1 and 2) have shown that the stresses and distortions in a swept wing can be appreciably different in character from those that would exist if the root were normal to the wing axis. The principal effect of sweepback on the stresses occurs under bending loads and consists in a concentration of bending stress and vertical shear in the rear spar near the fuselage. With regard to distortions, the effect of sweep is to produce some twist under loads that would produce only bending of an unswept wing and some bending under loads that would produce only twist of an unswept wing.

A relatively small amount of theoretical work has thus far been published on the analysis of swept wings of the shell type. Reference 3 presents an energy method for determining influence coefficients of a swept box beam with bulkheads parallel to the flight path, and references 1 and 2 contain a semiempirical method for the deflection analysis of a swept box beam with bulkheads perpendicular to the spars. No publications are known to be available on the stress analysis of a swept box beam with either type of bulkhead arrangement.

The purpose of this paper is to present a method for the calculation of both stresses and distortions of a swept box beam representing the main structural component of a swept wing with a carry-through section and with bulkheads perpendicular to the spars. The analysis is based on the four-flange idealized structure illustrated in figure 1. In a four-flange box beam of this type the carry-through and outer sections can be analyzed by existing methods for unswept four-flange box beams if some means is provided for analyzing the triangular section which connects them.

A method is presented for analyzing an idealized representation of the triangular section and for establishing continuity between the parts of the box beam; consideration is also given to the relationships between the idealized and actual structures and a comparison between the stresses and distortions calculated by this method and the experimental data of references 1 and 2. In the discussion, the effects of shear lag, which the method cannot give, are considered and an extension of the basic approach to permit their inclusion is indicated; also, the importance to the analysis of including the shear and bending flexibility of the bulkheads bordering the triangular region is demonstrated. A complete numerical example is worked out in an appendix.

SYMBOLS

Principal Concepts

A	area, square inches
a, a_n	length of bay, inches
a_{ij}	coefficients of matrix
B_n, C_n, D_n	arbitrary constants in solution of a differential equation
b	width of outer section, inches
b'	width of carry-through section, inches

c	depth of box beam or bulkhead, inches
E	modulus of elasticity, psi
F	force group statically equivalent to a bending moment, pounds
f,j,p	warping stiffness parameters
G	modulus of rigidity, psi
h	width of plate, inches
I	moment of inertia, inches^4
J	torsion constant, inches^4
k_i	stiffness factors of outer and carry-through sections
L	length of outer section, inches
l	length of beam, inches
M	bending moment, inch-pounds
N,N'	summations used in appendix B
P	axial load in flange or stringer, pounds
Q	area moment, inches^3
q	shear flow, pounds per inch
R	ratio which has the value +1 for symmetrical loads and -1 for antisymmetrical loads
T	torque, inch-pounds
t	sheet thickness, inches
U	strain energy, inch-pounds
u	displacement in the x direction, inches
V	vertical shearing force, pounds
w	downward displacement or deflection, inches
X	self-equilibrating, statically indeterminate force group, pounds

x,y,z	rectangular coordinates, inches
$\overline{y}$	distance from front spar to a specified center, inches
$\alpha,\beta,\delta,\epsilon,\omega$	stiffness factors of beams
γ	shear strain
ζ,η	nondimensional parameters used in discussion of idealization
θ	angle of twist, radians
Λ	angle of sweep, degrees
λ	effective width, inches
μ	Poisson's ratio (assumed to be 1/3)
ν	effectiveness factor
σ	normal stress, psi
τ	shear stress, psi
Φ	stress function
Ψ,ϕ	joint rotations, radians (see fig. 4)

Subscripts

Subscripts are used chiefly to designate the location of a dimension, force, or stress, as follows:

b	cover of the box beam
c	web of the box beam or bulkhead
F,f	front spar or flange (see fig. 7)
L	left-hand end of beam
l	along length of beam
l	value at $x = l$ } (appendix B)
o	value at $x = 0$ } (appendix B)

p plate

R,r rear spar or flange (see fig. 7)

R right-hand end of beam

x,y coordinate axis

s stringer

1,2,3...n specific locations shown in figures; also, numbers to identify stiffness factors

The single exception to the foregoing convention is:

e effective when applied to area, thickness, or moment of inertia

Superscripts

Superscripts are used to designate stresses and distortions produced by different types of action, as follows:

B bending

F F-force group

R rigid-body displacements

T torsion

W warping

X X-force group

σ flexure

τ shear

ANALYSIS OF THE IDEALIZED STRUCTURE

Basic Assumptions

The type of idealized structure analyzed is shown in figure 1. It is a four-flange box beam, which is considered swept back in order to

avoid ambiguity in the designation of the front and rear spars. The sweptback parts are made up of two triangular sections and two rectangular outer sections which are symmetrical about and continuous with a rectangular carry-through section representing the part of the wing within the fuselage. The outer and carry-through sections contain bulkheads which are placed perpendicular to the spars but the triangular section contains no bulkheads. All cross sections are symmetrical about a horizontal plane through the mid-depth of the spars.

The box beam is supported, either rigidly or elastically, at the four corners of the carry-through section so that the reactions are simple vertical forces. It is loaded by a series of vertical forces as shown in figure 1. The resulting stresses are within the elastic range.

The longitudinal direct stress in the idealized structure is assumed to be carried only by the concentrated areas at the corners of the cross section, and the side walls (spar webs) and covers are assumed to support shear stress only. The shear flow in the triangular cover sheets is assumed to be constant throughout the element (q_5 in fig. 2). This assumption implies the existence of uniformly distributed normal forces on the hypotenuse of the triangular cover sheet but, since the adjacent carry-through section can carry normal force only at its corners, these distributed forces are lumped into two statically equivalent concentrated forces (P_5 in fig. 2) at the ends of the hypotenuse. This assumption of uniform shear stress in the triangular sheet is approximately justified by the experimental data of references 1 and 2.

The two bulkheads which border the triangular section are assumed to be beams with finite shear and bending stiffness in their own plane but with no resistance to distortion out of their plane.

The relationship between the idealized structure described above and an actual structure is discussed subsequently.

Method of Analysis

The method of analysis is based on the assumption that the outer and carry-through sections can be analyzed by existing methods and that all that is then required is a means of establishing continuity between them through the triangular section. In order to accomplish this result, the structure is divided into a number of component parts as shown in figure 2. The forces assumed to exist on the cut sections are also shown.

The first step in the analysis is to consider the vertical edges of the triangular section (joints 1, 2, and 3) as free bodies (fig. 3) and to write equilibrium equations for them. These equations include two

for moment equilibrium and one for vertical shear equilibrium at each joint or a total of nine equations. The number of equations is considerably less than the number of unknown forces, and the problem is therefore statically indeterminate. The number of equations, however, is exactly equal to the number of displacements required to specify the attitude and position of the three joints. These displacements include two rotations and a vertical translation of each joint, as shown in figure 4.

The next step in the analysis, therefore, is to establish force-displacement relationships for each component of the structure shown in figure 2. Through these relationships the forces appearing in the equilibrium equations can be replaced by the joint displacements and the loads applied to the structure. The nine equilibrium equations then contain as unknowns only the nine joint displacements and can be solved simultaneously for the displacements. Once the joint displacements are known, the force-displacement relationships can be used again to determine the stresses and distortions of the entire structure.

If one, or both, of the bulkheads (1-3 or 2-3) is assumed rigid in its own plane, certain relationships among the joint displacements are immediately evident; thus the number of equilibrium equations needed is reduced and the analysis is simplified.

In an analysis of this type many of the factors involved depend upon the nature of the applied load (symmetrical or antisymmetrical, bending or torsion) and it may therefore be advantageous to make a separate analysis for each type of load and then superimpose the results to obtain the desired solution. For convenience in the detailed development which follows, however, provisions for both bending and torsion are included simultaneously but with restrictions that they are either symmetrical or antisymmetrical about the carry-through section.

Joint-Equilibrium Equations

If the three joints shown in figure 3 are considered as free bodies, a total of nine equilibrium equations can be written, two for moments and one for vertical shear at each joint, as follows:

Joint 1:

$$P_7 - P_5 - P_1 \cos \Lambda = 0 \tag{1}$$

$$P_9 + P_1 \sin \Lambda = 0 \tag{2}$$

$$V_1 + c(q_6 - q_9 - q_1) = 0 \tag{3}$$

Joint 2:

$$P_2 - P_{10} = 0 \tag{4}$$

$$P_{11} = 0 \tag{5}$$

$$V_2 + c\left(q_1 - q_2 - q_{10}\right) = 0 \tag{6}$$

Joint 3:

$$P_8 + P_4 \cos \Lambda - P_3 \sin \Lambda = 0 \tag{7}$$

$$P_6 - P_5 - P_4 \sin \Lambda - P_3 \cos \Lambda = 0 \tag{8}$$

$$V_3 + c\left(q_9 + q_{10} - q_8 + q_3\right) = 0 \tag{9}$$

Inasmuch as the number of unknown forces appearing is greater than the number of equations, the problem is statically indeterminate. The principle of consistent displacements will therefore be used to obtain a solution.

Force-Displacement Relations

The attitude and position of the joints can be completely described by nine joint displacements, two rotations, and a vertical translation at each joint (fig. 4). Thus the number of unknown joint displacements is exactly equal to the number of equilibrium equations, so that a solution is possible if sufficient force-displacement relations can be written to express all the unknown forces in terms of the nine joint displacements.

All the internal forces (P's and q's) shown in figure 2 can be expressed in terms of the unknown joint displacements and the loads applied to the outer section, with the use of the force-displacement relationships for each component of the structure. All that remain are the three vertical forces (V's) at the joints which are a combination of the vertical loads applied to the triangular section and the statically indeterminate support reactions. Since these forces are dependent upon the nature of each individual problem, they will be temporarily treated as known quantities; the modifications required for different types of supports are discussed in a subsequent section.

The force-displacement relationships for each component can be written as indicated in the following sections.

Beams.- The two bulkheads 1-3 and 2-3 and that part of the front spar 1-2 bordering the triangular section can be analyzed as beams subjected to end shears and moments plus a running shear along the flanges. This running shear results from the shear flows in the covers adjacent to the flanges. The loading and distortion of a beam of this type is illustrated in figure 5. In appendix A, this type of beam is analyzed and the following general expressions are obtained for the end loads in terms of the end displacements, the running shear, and certain stiffness parameters which include both the shear and bending resistance of the beam:

$$q_c = (\alpha - \beta)\frac{\phi_L + \phi_R}{l} + 2(\alpha - \beta)\frac{w_L - w_R}{l^2} - \epsilon q_l \tag{10}$$

$$P_L = -\alpha\phi_L + \beta\phi_R - (\alpha - \beta)\frac{w_L - w_R}{l} - \delta q_l \tag{11}$$

$$P_R = -\beta\phi_L + \alpha\phi_R + (\alpha - \beta)\frac{w_L - w_R}{l} + \delta q_l \tag{12}$$

where

$$\alpha = \frac{1}{\omega}\left(\frac{4}{3} + \frac{4EI}{Gctl^2}\right)$$

$$\beta = \frac{1}{\omega}\left(-\frac{2}{3} + \frac{4EI}{Gctl^2}\right)$$

$$\delta = \frac{1}{\omega}\left(\frac{2}{Gt}\right)$$

$$\epsilon = \frac{1}{\omega}\left(\frac{cl}{3EI}\right)$$

$$\omega = \frac{cl}{EI}\left(\frac{1}{3} + \frac{4EI}{Gctl^2}\right)$$

and

EI bending stiffness of beam

Gct shear stiffness of beam

Specific force-displacement relationships for each of the beams can be obtained by application of these general equations with the following results:

Front spar 1-2:

$$q_1 = (\alpha - \beta)_{12} \frac{\psi_1 \cos \Lambda + \phi_1 \sin \Lambda + \phi_2}{b \tan \Lambda} + 2(\alpha - \beta)_{12} \frac{w_1 - w_2}{b^2 \tan^2 \Lambda} + \epsilon_{12} q_5 \tag{13}$$

$$P_1 = -\alpha_{12}\left(\psi_1 \cos \Lambda + \phi_1 \sin \Lambda\right) + \beta_{12}\phi_2 - (\alpha - \beta)_{12} \frac{w_1 - w_2}{b \tan \Lambda} + \delta_{12} q_5 \tag{14}$$

$$P_2 = -\beta_{12}\left(\psi_1 \cos \Lambda + \phi_1 \sin \Lambda\right) + \alpha_{12}\phi_2 + (\alpha - \beta)_{12} \frac{w_1 - w_2}{b \tan \Lambda} - \delta_{12} q_5 \tag{15}$$

Bulkhead 1-3:

$$q_9 = (\alpha - \beta)_{13} \frac{\phi_1 - \psi_3 \cos \Lambda + \phi_3 \sin \Lambda}{b \sec \Lambda} + 2(\alpha - \beta)_{13} \frac{w_1 - w_3}{b^2 \sec^2 \Lambda} - \epsilon_{13}\left(q_7 + q_{11}\right) \tag{16}$$

$$P_9 = -\alpha_{13}\phi_1 - \beta_{13}\left(\psi_3 \cos \Lambda - \phi_3 \sin \Lambda\right) - (\alpha - \beta)_{13} \frac{w_1 - w_3}{b \sec \Lambda} - \delta_{13}\left(q_7 + q_{11}\right) \tag{17}$$

$$P_8 = -\beta_{13}\phi_1 - \alpha_{13}\left(\psi_3 \cos \Lambda - \phi_3 \sin \Lambda\right) + (\alpha - \beta)_{13} \frac{w_1 - w_3}{b \sec \Lambda} + \delta_{13}\left(q_7 + q_{11}\right) \tag{18}$$

Bulkhead 2-3:

$$q_{10} = -(\alpha - \beta)_{23} \frac{\psi_2 + \psi_3}{b} - 2(\alpha - \beta)_{23} \frac{w_3 - w_2}{b^2} + \epsilon_{23}\left(q_4 - q_5\right) \tag{19}$$

$$P_4 = -\alpha_{23}\psi_{23} + \beta_{23}\psi_2 - (\alpha - \beta)_{23} \frac{w_3 - w_2}{b} - \delta_{23}\left(q_4 - q_5\right) \tag{20}$$

$$P_{11} = -\beta_{23}\psi_3 + \alpha_{23}\psi_2 + (\alpha - \beta)_{23} \frac{w_3 - w_2}{b} + \delta_{23}\left(q_4 - q_5\right) \tag{21}$$

In these equations the subscripts 12, 13, and 23 applied to the stiffness parameters α, β, δ, and ϵ refer to the front spar 1-2 and the two bulkheads 1-3 and 2-3, respectively. Several unknown forces, namely, q_4, q_5, q_7, and q_{11}, which do not occur in the joint equilibrium equations, appear on the right-hand sides of equations (13) to (21); these forces, too, can be expressed in terms of the nine joint displacements when the other structural components are considered.

Triangular cover sheet.- The triangular cover sheet is assumed to carry a uniform shear flow q_5 along its mutually perpendicular edges (1-2 and 2-3). In order that this element be in equilibrium, shear and normal stresses are required along the hypotenuse and the corresponding forces are shown (fig. 2) as a uniform shear flow q_{11} acting along that edge and a pair of concentrated forces P_5 acting at the joints. The equilibrium equations are:

$$q_{11} = -q_5 \cos 2\Lambda \tag{22}$$

$$P_5 = -q_5 b \sin \Lambda \tag{23}$$

Force-displacement relationships are obtained by assuming that the maximum shear strain in the sheet is equal to the amount by which the right angle 1-2-3 is changed. In terms of the joint rotations, this shear strain is:

$$\gamma_{1\text{-}2\text{-}3} = \frac{c}{2}\left(\frac{\psi_1 \sin \Lambda - \phi_1 \cos \Lambda - \psi_2}{b \tan \Lambda} + \frac{\phi_3 - \phi_2}{b}\right) \tag{24}$$

Then,

$$q_5 = \frac{Gtc}{2b}\left(\psi_1 \cos \Lambda - \psi_2 \cot \Lambda - \phi_1 \cos \Lambda \cot \Lambda - \phi_2 + \phi_3\right) \tag{25}$$

and the relations for q_{11} and P_5 follow immediately from equations (22) and (23).

Outer section.- That part of the structure outboard of bulkhead 2-3 acts as an unswept cantilever box beam supported on a flexible root and, as such, can be analyzed by existing methods of analysis. The stresses and distortions at any point can be expressed in terms of the applied loads, the distortions of the root, and certain elastic stiffness factors. Then, the force-displacement relationships required to define the internal forces at the root are:

$$P_3 = k_1M - k_2T + k_3(\phi_2 - \phi_3) \tag{26}$$

$$P_{10} = k_4M + k_2T - k_3(\phi_2 - \phi_3) \tag{27}$$

$$q_2 = k_5V + k_6T + k_7(\phi_2 - \phi_3) \tag{28}$$

$$q_3 = -k_{10}V + k_6T + k_7(\phi_2 - \phi_3) \tag{29}$$

$$q_4 = k_8V + k_9T - k_7(\phi_2 - \phi_3) \tag{30}$$

In these equations V, M, and T represent, respectively, the applied vertical shear, bending moment, and torque (about some reference axis) at the root of the outer section and the k's represent elastic stiffnesses of the outer section. The stiffness factors k_1, k_2, k_4 and the like are functions of the distribution of the applied loads and the dimensions and material of the outer section, whereas k_3 and k_7 depend only on the latter. The quantity $\phi_2 - \phi_3$ is a measure of the warping of the root cross section and is the only root distortion appearing in the equations, since the others are rigid-body movements which do not affect the stress distribution. Thus, effectively, the root bulkhead is assumed rigid in its own plane as far as the outer-section analysis is concerned.

Any method of analysis can be used to determine the stiffness factors provided that cross-sectional warping and its restraint are taken into account. This provision requires a more refined approach than is made in elementary bending theory. The stiffness factors are the same for symmetrical and antisymmetrical loadings but, since bending and torsion produce different types of effects, they have been separated in the equations. In order to evaluate the torque T, the loads must be referred to a reference axis. The most desirable axis is one which makes the stresses at the root due to the bending moment M equivalent to those given by elementary theory, although it is not generally possible to achieve this relationship at all stations. The so-called "shear center" does not locate such an axis. The choice of a reference axis will be treated at greater length in the section on idealization.

Carry-through section.- The carry-through section, like the outer section, is a box beam that can be analyzed by existing methods. In this case, however, the stress distribution is expressed in terms of only the end distortions since internal end forces are the only loads applied. The force-displacement relationships are then:

$$P_6 = k_{11}(\psi_1 + \psi_3 \sin\Lambda + \phi_3 \cos\Lambda) + k_{12}(\psi_1 - \psi_3 \sin\Lambda - \phi_3 \cos\Lambda) + k_{13}(w_1 + w_3) + k_{14}(w_1 - w_3) \tag{31}$$

$$P_7 = k_{15}\left(\psi_1 + \psi_3 \sin\Lambda + \phi_3 \cos\Lambda\right) + k_{16}\left(\psi_1 - \psi_3 \sin\Lambda - \phi_3 \cos\Lambda\right) + k_{17}\left(w_1 + w_3\right) + k_{18}\left(w_1 - w_3\right) \tag{32}$$

$$q_6 = k_{19}\left(\psi_1 + \psi_3 \sin\Lambda + \phi_3 \cos\Lambda\right) + k_{20}\left(\psi_1 - \psi_3 \sin\Lambda - \phi_3 \cos\Lambda\right) + k_{21}\left(w_1 + w_3\right) + k_{22}\left(w_1 - w_3\right) \tag{33}$$

$$q_7 = k_{23}\left(\psi_1 + \psi_3 \sin\Lambda + \phi_3 \cos\Lambda\right) + k_{24}\left(\psi_1 - \psi_3 \sin\Lambda - \phi_3 \cos\Lambda\right) + k_{25}\left(w_1 + w_3\right) + k_{26}\left(w_1 - w_3\right) \tag{34}$$

$$q_8 = k_{27}\left(\psi_1 + \psi_3 \sin\Lambda + \phi_3 \cos\Lambda\right) + k_{28}\left(\psi_1 - \psi_3 \sin\Lambda - \phi_3 \cos\Lambda\right) + k_{29}\left(w_1 + w_3\right) + k_{30}\left(w_1 - w_3\right) \tag{35}$$

In these equations, the k's represent elastic stiffness factors, which depend upon whether the loading is symmetrical or antisymmetrical, as well as upon the dimensions and material of the carry-through section. They may be determined by any method of analysis as long as cross-sectional warping and the shear and bending stiffness of the spars are considered. The displacements which appear have been so grouped that they have a particular physical meaning. Thus, the quantities associated with the first, second, third, and fourth terms in parentheses represent a bending type of rotation, a warping, a translation, and a torsion type of rotation of the end cross section, respectively.

Solving for the Joint Displacements

The force-displacement relationships (equations (13) to (35)) are sufficient to express all the internal forces in the equilibrium equations in terms of the nine basic joint displacements and the applied loads. Upon substitution, the nine equations involve only nine unknown displacements; namely, ψ_1, ψ_2, ψ_3, ϕ_1, ϕ_2, ϕ_3, $\frac{w_1}{b}$, $\frac{w_2}{b}$, and $\frac{w_3}{b}$; and they can then be solved numerically for these unknowns.

The equations obtained by direct substitution have coefficients containing many terms which are tedious to evaluate; however, a number

of combinations can be made which substantially simplify the final equations. Equations (1) to (9) are combined as follows to obtain nine simpler equations:

$$\left[(1) - (8)\right] \sec \Lambda - (4) + (5) \tan \Lambda \tag{36}$$

$$\left[(2) + (7)\right] \csc \Lambda + (4) + (5) \cot \Lambda \tag{37}$$

$$\frac{1}{c}\left[(3) + (6) + (9)\right] \tag{38}$$

$$(4) \tag{39}$$

$$(5)\frac{1}{\delta_{23}} \tag{40}$$

$$\frac{b}{c}(6) \tan \Lambda \tag{41}$$

$$(7) \sec \Lambda + (5) \tag{42}$$

$$(8) \sec \Lambda - (5) \tan \Lambda \tag{43}$$

$$\frac{b}{c}(9) \sec \Lambda \tag{44}$$

The resulting system of equations is written in matrix form as follows:

$$\begin{bmatrix} a_{11} & a_{12} & a_{13} & a_{14} & a_{15} & a_{16} & a_{17} & a_{18} & a_{19} \\ a_{21} & a_{22} & a_{23} & a_{24} & a_{25} & a_{26} & a_{27} & a_{28} & a_{29} \\ a_{31} & a_{32} & a_{33} & a_{34} & a_{35} & a_{36} & a_{37} & a_{38} & a_{39} \\ a_{41} & a_{42} & a_{43} & a_{44} & a_{45} & a_{46} & a_{47} & a_{48} & a_{49} \\ a_{51} & a_{52} & a_{53} & a_{54} & a_{55} & a_{56} & a_{57} & a_{58} & a_{59} \\ a_{61} & a_{62} & a_{63} & a_{64} & a_{65} & a_{66} & a_{67} & a_{68} & a_{69} \\ a_{71} & a_{72} & a_{73} & a_{74} & a_{75} & a_{76} & a_{77} & a_{78} & a_{79} \\ a_{81} & a_{82} & a_{83} & a_{84} & a_{85} & a_{86} & a_{87} & a_{88} & a_{89} \\ a_{91} & a_{92} & a_{93} & a_{94} & a_{95} & a_{96} & a_{97} & a_{98} & a_{99} \end{bmatrix} \begin{bmatrix} \psi_1 \\ \psi_2 \\ \psi_3 \\ \phi_1 \\ \phi_2 \\ \phi_3 \\ \frac{w_1}{b} \\ \frac{w_2}{b} \\ \frac{w_3}{b} \end{bmatrix} = \begin{bmatrix} a_{10} \\ a_{20} \\ a_{30} \\ a_{40} \\ a_{50} \\ a_{60} \\ a_{70} \\ a_{80} \\ a_{90} \end{bmatrix} \tag{45}$$

The coefficients a_{ij} are given by the expressions in table I.

The terms in the matrix of coefficients involve the elastic stiffness factors and dimensions of the structure; the constant terms contain elastic stiffness factors, the loads applied to the outer section, and the vertical forces at the joints. Each of these joint forces contains a component of the load applied to the triangular section and, in addition, V_1 and V_3 contain the support reactions which may be statically indeterminate. The loads applied to the triangular section are so divided among the three vertical edges that the resulting forces form a statically equivalent system. The reactions depend upon the nature of the supports and are introduced into the analysis as indicated in the following sections.

Rigid supports.- In the case of rigid supports w_1 and w_3 are zero and there are thus seven unknown joint displacements which require only seven equations for their determination. In the matrix, equation (45), columns 7 and 9, which are the coefficients of w_1 and w_3, respectively, can be immediately eliminated. The required seven equations are then obtained by the elimination of two rows, the logical ones being rows 3 and 9 since they are derived from equations containing the unknown support reactions. After the joint displacements have been calculated, V_1 and V_3 can be determined by substitution into equations (3) and (9).

Elastic supports.- For the case of elastic supports, all nine equations are required but must be modified to include force-displacement relationships for the supports. The joint forces can be expressed as follows:

$$V_1 = k_{31}w_1 + V_1'$$

$$V_3 = k_{32}w_2 + V_3'$$

where

k support stiffness factor

V' component of loads applied to triangular section

Calculating Stresses and Distortions Throughout the Idealized Structure

The stress and distortion distributions for the complete box beam have been defined in terms of the applied loads and the nine joint displacements. Once these joint displacements have been determined by solving equation (45), the procedures outlined previously can be reversed and all of the forces at the joints can be calculated.

Determination of the detailed distributions is slightly more complicated. For the front spar and the two bulkheads bordering the triangular section, the equations of appendix A can be used. For the outer and carry-through sections, the complete stress distribution can be determined from the analysis that was used to obtain the stiffness factors k_1 to k_{30}. The effects of rigid body motions, which do not affect the stresses, must be included in the calculation of distortions.

The relationships between the computed stresses in the idealized structure and the actual structure are discussed in the section on idealization, which follows.

IDEALIZATION OF AN ACTUAL STRUCTURE

Outer and Carry-Through Sections

The outer and carry-through sections are unswept box beams which can be analyzed by existing methods of analysis. Since such methods are by no means standard, however, a definite procedure is presented in order that the idealization of the complete structure may follow a consistent pattern.

The basic assumption that the idealized outer and carry-through sections are conventional four-flange boxes implies that the normal stress in the walls of the actual box beam varies linearly between adjacent corners. A generalized stress distribution of this type can be represented by a linear combination of the two stress distributions shown in figure 6(a), one of which equilibrates the applied load and is uniform across the cover, while the other is self-equilibrating and varies linearly across the cover. The uniform distribution is designated bending stress because it is obtained from elementary beam theory which assumes that plane cross sections remain plane after loading. Similarly, the linearly varying stress is designated warping stress because it is associated with the warping of the cross section out of its plane.

The normal stresses on the actual cross section are represented by four concentrated forces at the corners of the idealized cross section. The total force at each corner consists of two components, one from the F-force group corresponding to the bending-stress distribution and one from the X-force group corresponding to the warping-stress distribution, as shown in figure 6(b). The equivalence between the force group and the corresponding distributed stress is determined on the basis of overall statics of the cross section and the moment applied to each cover. The effective flange areas of the idealized structure are then chosen so that the flange stress in the idealized structure is equal to the corner stress in the actual structure.

A cross section of the type shown in figure 7(a) can then be idealized as follows:

(1) Obtain the equivalent cover (fig. 7(b)) by adding, to the actual cover and corner flanges, areas representing the moment-carrying capacity of the webs; that is, $\frac{1}{6}ct_r$ and $\frac{1}{6}ct_f$; the area of the equivalent cover is therefore:

$$A_b = A_f + \frac{1}{6}ct_f + A_r + \frac{1}{6}ct_r + bt_b + \sum_n (A_s)_n \tag{46}$$

(2) Locate the centroid of the equivalent cover:

$$\frac{\bar{y}}{b} = \frac{1}{A_b}\left\{\frac{1}{2}bt_b + A_r + \frac{1}{6}ct_r + \sum_n \left(A_s \frac{y}{b}\right)_n\right\} \tag{47}$$

(3) Calculate the moment of inertia of the equivalent cover about a vertical axis through its centroid:

$$\frac{I_b}{b^2} = \left(A_f + \frac{1}{6}ct_f\right)\left(\frac{\bar{y}}{b}\right)^2 + \left(A_r + \frac{1}{6}ct_r\right)\left(1 - \frac{\bar{y}}{b}\right)^2 + \frac{1}{12}bt_b + bt_b\left(\frac{1}{2} - \frac{\bar{y}}{b}\right)^2 + \sum_n A_{s_n}\left(\frac{y_n}{b} - \frac{\bar{y}}{b}\right)^2 \tag{48}$$

(4) The effective area of each front flange is then:

(a) For bending stresses:

$$A_F^B = \left(1 - \frac{\bar{y}}{b}\right)A_b = \left(1 - \frac{\bar{y}}{b}\right)\frac{2I}{c^2} \tag{49}$$

where I is the moment of inertia of the entire cross section about the horizontal axis of symmetry.

(b) For warping stresses:

$$A_F^W = \frac{I_b/b^2}{\bar{y}/b} \tag{50}$$

(5) The effective area of the rear flange in each case is:

$$\left.\begin{aligned} A_R^B &= A_F^B \frac{\frac{\bar{y}}{b}}{1 - \frac{\bar{y}}{b}} \\ A_R^W &= A_F^W \frac{\frac{\bar{y}}{b}}{1 - \frac{\bar{y}}{b}} \end{aligned}\right\} \tag{51}$$

If many equally spaced stringers are used, satisfactory results can be obtained by treating them as an equivalent sheet and thus eliminating the evaluation of lengthy summations.

It is important to note that a different effective area is associated with each type of stress distribution, as should be expected, since each is associated with a different type of physical action; therefore, if accurate results are to be obtained, the two types of stress distributions must be completely separable in the analysis, that is, they do not appear simultaneously in the evaluation of any one stiffness factor in equations (26) to (35). This separation is not generally possible; however, one way to accomplish complete separation in the outer section will be described. Similar considerations apply to the carry-through section.

The outer section is an unswept cantilever box beam on a flexible root and the forces on any cross-section as given in equations (26) to (30) can be expressed as the sum of: (1) forces that exist in the loaded cantilever on a rigid root and (2) forces that exist in an unloaded cantilever having the root warped an amount $(\phi_2 - \phi_3)$. Since root warping produces only warping stresses, the effective areas for warping stresses (equations (50) and (51)) are used for the determination of the stiffness factors k_3 and k_7. The choice of effective areas for the analysis of the loaded cantilever is more difficult because the application of vertical loads will, in general, produce both bending and warping stresses; however, since torque loads produce only warping stresses, it may be possible to locate some axis along which applied vertical loads will produce only bending stresses at every cross section; then, the loading can be divided into vertical forces applied along this axis and torques about this axis. The stress types are thus separated and the effective areas for bending stress (equations (49) and (51)) can be used to calculate the stiffness factors associated with the vertical loads $(k_1, k_4, k_5, k_8$ and $k_{10})$ and the effective areas for warping

stresses (equations (50) and (51)) can be used to calculate the stiffness factors $(k_2, k_6, \text{and } k_9)$ associated with the torque.

An axis of the type described obviously exists for a doubly symmetrical cross section; such an axis is also known to exist for a four-flange box beam of constant cross section which is symmetrical about a horizontal plane (fig. 7(c)). The location of this axis, at the center which might be called the zero warping center of the cross section, is given by:

$$\frac{y}{b} = \frac{\bar{y}}{b}\zeta + \frac{t_c}{2t_f}(1 - \zeta) \tag{52}$$

where

$$\frac{1}{t_c} = \frac{1}{2}\left(\frac{1}{t_f} + \frac{1}{t_r}\right)$$

$$\zeta = \frac{\frac{b}{t_b} + \frac{c}{t_c}}{\frac{b}{t_b} - \frac{c}{t_c}}$$

The zero warping center should not be confused with the shear center. Vertical loads applied along an axis through the shear center will deflect the box beam without twisting it, if the cross sections are free to warp, a condition that is not satisfied at the rigid root of a cantilever. Vertical loads applied along an axis through the zero warping center will result in a combination of deflection and twist, but the cross sections of the box will not warp. If the cross-section is doubly symmetrical, the zero warping center and shear center coincide at the geometrical center of the cross section.

The preceding discussion has been exclusively concerned with the problem of converting the actual structure into an idealized structure that can be easily analyzed. After the analysis has been completed and the magnitudes of the corner forces determined, the problem of converting corner forces into stress distributions arises. This conversion of forces is accomplished by determining the stresses corresponding to each type of force group (F or X) and then summing the stresses to get the total stress. The relationship between force groups and stress distributions are shown in figure 6. The type of force group is determined from physical considerations; for example, equation (26) shows that P_3 is composed of three forces of which k_1M is of the bending type whereas k_2T and $k_3(\phi_2 - \phi_3)$ are of the warping type.

With regard to shear stresses, the analysis of the idealized structure gives the average value of the shear flows in the walls of the actual structure. A more detailed shear-stress distribution can be derived from the distributed normal stresses; however, this additional refinement is probably unwarranted in view of the many approximations in the basic solution.

Triangular Section

The idealized triangular section consists of three parts: the two cover sheets which are in a state of uniform shear, and the front spar, which is assumed to be a beam.

The thickness assigned to the idealized cover sheet should properly represent the shear stiffness of the actual cover. For unbuckled sheet alone, this thickness is that of the actual sheet. This value should be decreased if the sheet has buckled or increased if there are closed-section stringers which contribute to its shear resistance. Similar considerations apply to the determination of the shear resistance of any other element of the structure.

In the calculation of the moment of inertia of the front spar, a contribution from the sheet and stringers in the cover of the triangular section must be included to account for their ability to carry direct stress. For simplicity, the moment of inertia of the idealized front spar is assumed constant in the spanwise direction and thus may be determined by treating the triangular bay as a rectangular bay of constant cross section equal in width to the triangular bay where it joins the outer section; an effective area may then be assigned to the idealized front spar by the method recommended for the outer section. This idealization will result in two moments of inertia, one for bending and one for warping stress. Again, separation of these two stress systems in the analysis is desirable but in this case it is only partly possible. If the load on the outer section is torsion only, only warping stress will exist in the triangular section and the effective warping area should be used. If the loads on the outer section are of the bending type only, both kinds of stresses will exist in the triangular section and direct separation is impossible; however, the warping stress is usually small compared with the bending stress and in such cases satisfactory results can be obtained by using the effective bending area.

Bulkheads

When values of flexural stiffness are assigned to the two bulkheads bordering the triangular section, consideration must be given to the fact that bending of these beams is accompanied by extension or

compression of the adjacent cover sheets. The analysis in appendix B gives the distortions of a combined bulkhead and cover sheet and the moment of inertia of a simple bulkhead which has the same distortion. The results can be summarized as follows:

$$I_e = I(1 + \nu) \tag{53}$$

where

I moment of inertia of bulkhead alone, inches^4

I_e effective moment of inertia of combination, inches^4

ν an effectiveness factor plotted in figure 8 as a function of the nondimensional parameter $\left(\frac{c^2 l t_e}{I}\right)$

c depth of bulkhead, inches

l length of bulkhead, inches

t_e equivalent thickness of the cover sheet, inches $\left(t \frac{E_{sheet}}{E_{bulkhead}}\right)$

E modulus of elasticity, psi

COMPARISON BETWEEN THEORY AND EXPERIMENT

The accuracy of the method is demonstrated by comparing calculated stresses and distortions with the test data of references 1 and 2. The test specimen used is illustrated in figures 9 and 10 and the details of the calculations are given in the numerical example of appendix C. The comparisons are presented graphically for each of the four test conditions, symmetrical and antisymmetrical tip bending and torsion loads as follows:

(a) Distortions of the outer section in figure 11

(b) Spanwise distribution of spar shear stresses shown in the left-hand parts of figure 12

(c) Spanwise distribution of flange normal stresses shown in the right-hand parts of figure 12

(d) Chordwise distributions of normal stress at three spanwise stations in figure 13

In each case the sign conventions employed are those of references 1 and 2 which are occasionally in conflict with those employed elsewhere in this paper.

The test data in these figures are presented in the usual manner and several calculated curves are given to illustrate different theoretical approaches, as follows:

(a) All figures contain a heavy solid line which represents the results of the numerical example of appendix C. The area under this curve is vertically hatched in the stress plots (figs. 12 and 13).

(b) A dash-dot line appears in some figures to show the effect of superimposing shear-lag effects on the results of the numerical example. The determination of these effects is described in the discussion.

(c) The stress plots also contain dash lines which give results obtained from elementary theory $\left(\frac{Mc}{I}, \frac{VQ}{It}, \text{and } \frac{T}{2At}\right)$.

In general, the results of the numerical example (solid lines) are in fair agreement with the test data; however, much better agreement is achieved when shear-lag effects are added where applicable. Elementary theory gives the least satisfactory results since it does not include the effects of either sweep or shear lag. The discrepancies between the calculations of the numerical example and the experimental data are primarily the result of analyzing an overly simplified idealization of the actual structure. The assumed idealized structure is incapable of distorting in all of the shapes assumed by the actual box beam; therefore, the analysis cannot give completely accurate results. The most significant effect of oversimplification is the neglect of shear-lag stresses. Shear lag appears whenever the webs carry vertical shear stress and it is characterized by an increase in normal stress in the vicinity of the flanges with a corresponding decrease in the rest of the cover (see fig. 14). There is also an associated change in the shear stresses in the cover.

The effect of shear lag on the stress distribution is most evident in the chordwise plots of figure 13. It appears in the outer section for the bending loads and in the carry-through section for the antisymmetrical loads. In each case the effect is carried over into the triangular section because of continuity.

Shear-lag stresses effectively reduce the stiffness of the structure and thus increase its deflection. The cantilever beam deflection of the outer section is increased by its own shear lag, but for this specimen the increase was small enough to be neglected. More important is the reduced stiffness of the carry-through section under antisymmetrical

loads which results in an increased rotation of the ends of the carry-through section. This effect causes only a rigid-body rotation of the triangular and outer sections since the carry-through section is doubly symmetrical. The effect of shear lag in the carry-through section was estimated by reducing the moment of inertia of the carry-through section ($I_e = 0.252I$) by the procedure described subsequently in the "Discussion" with the results shown in figure 11(b) and 11(d). For the antisymmetrical bending load the effect was underestimated whereas it was overestimated for the antisymmetrical torsion load.

Some other effects of oversimplification are associated with the idealization of the triangular section. The actual structure had a short bulkhead (bulkhead 7, fig. 9) in the triangular section which was neglected in the analysis. Its presence introduces additional restraints which change the shear stress in the front spar (fig. 12) and the chordwise normal-stress distributions in the carry-through section (fig. 13). Also, a number of approximations were used with regard to the effective moment of inertia of the front spar which introduce uncertainties in the analysis.

Another factor that affects the agreement is the flexibility of the supporting jig used in the tests. This jig was assumed rigid in the analysis but deflected during the tests. Under symmetrical loads (reference 1) these deflections amounted to a rigid-body rotation of the complete structure and it was a simple matter to correct the measured deflections; however, under antisymmetrical loads, a small amount of twist remained in the carry-through section after the rigid-body corrections had been made (reference 2). The method of analysis developed in this paper was used to calculate the effect of the measured carry-through section twist on the theoretical stresses and deflections. For the antisymmetrical bending load the principal changes were in the shear stresses in the carry-through section, as might be expected, because of the torque required to twist this section. The warping stresses also changed throughout the box beam and the deflection of the outer section increased. For the antisymmetrical torsion load the twist was small enough to be negligible. In general, these changes improved the agreement between theory and experiment but were not of sufficient magnitude to warrant their addition to the calculated results.

DISCUSSION

Determination of Shear-Lag Effects

The method presented in this paper is for the analysis of a four-flange box beam which experiences only first-order warping. Thus, the stress distribution in the actual structure varies linearly between

corners and consists of the bending and warping stress components shown in figure 6. An actual structure experiences other types of cross-sectional warping, a common one being the second-order or shear-lag type which introduces a departure from linearity in the cover stresses by superimposing a self-equilibrating stress distribution of the type shown in figure 14(a). The experimental data of references 1 and 2 show that shear lag is important in the specimen tested because it causes an increase in the flange normal stresses which is, in some cases, larger than the changes caused by first-order warping and increases the flexibility of the structure which increases the deflections. Some means for calculating these effects is therefore necessary.

Any method used to calculate shear-lag effects requires the analysis of a more complicated idealized structure than the four-flange box beam. Conforming to the previous assumptions regarding the stress-carrying ability of the idealized structure, the minimum addition is a single central stringer in each cover as shown in figure 14(b); other additional cover stringers permit calculation of the effects of third and higher order warping. These more complicated structures can be introduced into the analysis in either of two ways: (1) The basic method can be extended to the direct analysis of the more complicated structure and thus automatically include shear-lag effects. (2) The results of the simpler analysis can be corrected by a process which combines experimental data and individual shear-lag analyses of the outer and carry-through section. Each of these approaches is briefly described.

The direct extension of the basic method involves the analysis of an idealized structure of the type shown in figure 15. The analysis follows the procedure previously described but two new features are introduced. First, more joints are involved, for which additional equilibrium equations are required and thus a larger system of simultaneous equations must be solved. Second, force-displacement relationships for the outer, triangular, and carry-through sections must be modified to account for the new types of forces and distortions of the idealized structure.

The correction process can take on a variety of forms, two of which were used to calculate the shear-lag corrections applied to the results of the numerical example, appendix C, to obtain the dash-dot lines in figures 11, 12, and 13. The shear-lag corrections for the outer section were determined by using the single-substitute stringer method (reference 4) to calculate the shear-lag stresses in the outer section. The outer section was analyzed as an ordinary, unswept box beam on a rigid root and a constant empirical multiplying factor was used to obtain good over-all agreement with the experimental spanwise and chordwise normal-stress distributions. The multiplying factor accounts for the root restraint provided the outer section by the triangular section;

this factor was found to be 0.77 for the symmetrical bending load and 1.28 for the antisymmetrical bending load.

A somewhat different procedure was used to determine the shear-lag corrections for the carry-through section because it was found that the shear-lag stresses, caused by the antisymmetrical bending load, could be approximated by a shear-lag analysis which assumed that the end cross sections were restrained from warping. This approach, however, was less satisfactory for the antisymmetrical torque load. The method used analyzed the cover as an equivalent sheet which carried both shear and normal stress (reference 5) and it gave better chordwise and spanwise stress distributions than a similar analysis which used the single substitute stringer method. The reduced moment of inertia used to determine the effect of shear lag on the distortions of the carry-through section was also obtained from this analysis.

From considerations of accuracy, the preferred method for the determination of shear-lag effects is the direct extension to a more complicated idealized structure; however, such an analysis requires a large amount of work. The ease with which the correction process can be used is a definite advantage, but it can be applied, with assurance of accuracy, only to structures closely resembling the test specimen from which the empirical factors were obtained. Even then, the correction process is only fairly accurate because it cannot adequately account for the interaction between the various parts of the structure.

Effects of Bulkhead Flexibility

In the analysis of unswept box beams the internal bulkheads are often assumed to be rigid in their own plane. This assumption yields satisfactory results except when a discontinuity of structure or loading, such as a cut-out, introduces large loads into a bulkhead. A study of the test results presented in references 1 and 2 shows that bulkheads 6 and 8 (fig. 9) of the test specimen were subjected to substantial shear and bending loads; thus, their distortions may have an important effect on the structure. The shear and bending flexibility of the bulkheads bordering the triangular section is included as a basic feature of the method of analysis presented in this paper although the development could have been considerably simplified by assuming them rigid.

The effect of bulkhead flexibility on the stress and distortions of the swept box beam of references 1 and 2 was investigated by solving a series of numerical examples similar to that of appendix C. These examples were for symmetrical tip bending and torque loads for the four cases of bulkhead flexibility listed in the following table (all bulkheads other than bulkheads 1-3 and 2-3 (fig. 2) were assumed rigid):

Case	Bulkhead 1-3	Bulkhead 2-3
I	Flexible	Flexible
II	Flexible	Rigid
III	Rigid	Flexible
IV	Rigid	Rigid

Selected stresses and displacements calculated for each case are compared in figure 16. Despite the fact that the bulkheads were constructed of $\frac{1}{8}$-inch steel plate, appreciable errors occurred when they were assumed rigid in their own plane. The effects of bulkhead flexibility on the stresses were more pronounced for torsion than for bending loads; however, for each type of load the solution for case IV overestimated the warping stress in the outer section. The different root distortions calculated for each of the four cases lead to slightly different deflections and somewhat greater differences between the rotations of the outer section.

In general, the results indicate that the flexibility of the bulkheads bordering the triangular section has an important effect upon the stresses and distortions of a swept box beam and should be considered in the analysis if accurate results are to be obtained.

In addition to the studies of bulkhead flexibility, some investigations were made of the effect of the number of bulkheads in the triangular section. For example, a numerical analysis which used the assumption of closely spaced rigid bulkheads, often used in shell analysis, gave very erroneous results for the stress distribution in the triangular section. In all the cases considered, the number of bulkheads in the triangular section had only a small effect on the stresses outside of the triangular section. The experimental data in figures 12 and 13 illustrate the effect of an extra bulkhead on the stresses within the triangular section.

Extension of the Method

The method of analysis in the form presented, is not expected to be generally applicable to the precise analysis of all swept wings because of differences in structural arrangement and the degree of idealization assumed; however, the basic approach can be used in many situations.

Extension of the method to other types of swept wings is straight forward if the bulkheads are perpendicular to the spars. The modifications required to obtain more accurate stress distributions have been

indicated in the section on the determination of shear-lag effects. Similar procedures are required for the analysis of multispar box beams, that is, additional joints are created where the spars cross the bulkheads.

Application of the basic approach to swept box beams in which the bulkheads are placed parallel to the flight direction introduces some new problems. In the first place, a swept wing of this type does not have an outer section which can be analyzed by existing methods. Extension of the method of joints, which is a feature of the basic approach, to the entire structure substantially increases the complexity of the solution and some other approach may be more desirable. A second problem is the establishment of force-displacement relationships which correctly predict the physical behavior of the parallelogram-shaped cover sheets.

CONCLUDING REMARKS

A method has been described for the stress and distortion analysis of a swept box beam with a carry-through section and with bulkheads perpendicular to the spars. The method is based on a simple four-flange box type of idealized structure and permits an estimation of the first-order warping stresses that result from sweep but does not permit the evaluation of higher-order stresses such as shear lag. Agreement with experiment is therefore only fair; however, extension of the basic approach to permit more refined analyses, which include shear-lag effects and other structural arrangements such as multiple spars, has been indicated.

The method assumes that the outer and carry-through sections are unswept box beams and thus can be analyzed by existing methods. Continuity is established between them through the analysis of the triangular section. The analysis of the triangular section isolates the structural joints as free bodies and gives an equilibrium equation for each degree of joint freedom. The joint forces are expressed in terms of joint displacements and a set of simultaneous linear equations, which completely defines the joint displacements, is thus obtained.

The method takes into account the flexibility, both as regards shear and bending, of the bulkheads in and around the triangular section. The results of a numerical study have been presented to show that

appreciable errors can appear in the calculated stresses and deflections if the usual assumption of rigid bulkheads is used in this region.

Langley Aeronautical Laboratory
National Advisory Committee for Aeronautics
Langley Air Force Base, Va., August 17, 1950

APPENDIX A

FORCE-DISPLACEMENT RELATIONSHIPS FOR BEAMS

The beam analyzed is assumed to be of constant idealized cross section with a web which carries only shear stress and subjected to the loading shown in figure 5(a). This loading consists of flange axial loads P_L and P_R at the ends of the beam, a constant running shear flow q_l applied to the flanges and a constant shear flow q_c in the web. The distorted shape of the beam under load can be described by the end displacements w_L and w_R and the end rotations ϕ_L and ϕ_R (fig. 5(b)).

Consideration of a differential element of the beam (fig. 5(c)) yields the following equilibrium equation

$$\frac{dP}{dx} - q_l - q_c = 0 \tag{A1}$$

and the following relations between loads and distortion

$$q_c = Gt\left(\phi - \frac{dw}{dx}\right) \tag{A2}$$

$$P = \frac{EI}{c}\frac{d\phi}{dx} \tag{A3}$$

Substituting equations (A2) and (A3) in (A1) yields

$$\frac{dw}{dx} = -\frac{EI}{Gct}\frac{d^2\phi}{dx^2} + \phi + \frac{q_l}{Gt} \tag{A4}$$

and, since q_c is constant, from equation (A2),

$$\frac{d\phi}{dx} = \frac{d^2w}{dx^2} \tag{A5}$$

Equations (A4) and (A5) have solutions which can be expressed as follows:

$$\phi = C_1 + C_2x + C_3x^2 \tag{A6}$$

$$w = C_1x + \frac{1}{2}C_2x^2 + C_3\left(\frac{1}{3}x^3 - \frac{2EIx}{Gct}\right) + C_4 + \frac{q_l}{Gt}x \tag{A7}$$

where C_1, C_2, C_3, C_4 are constants which can be determined from the boundary conditions. In this case, the boundary conditions are prescribed as follows:

$$\left.\begin{aligned} w_{x=o} &= w_L \\ w_{x=l} &= w_R \\ \phi_{x=o} &= \phi_L \\ \phi_{x=l} &= \phi_R \end{aligned}\right\} \tag{A8}$$

These boundary conditions require that the constants C_n have the following values:

$$\left.\begin{aligned} C_1 &= \phi_L \\ C_2 &= \frac{1}{l}\left(\phi_R - \phi_L\right) - C_3 l \\ C_3 &= -\frac{1}{2l}\left[\frac{2\left(w_R - w_L\right) - l\left(\phi_R + \phi_L\right) - \frac{2l}{Gt}q_l}{\frac{l^2}{6} + \frac{2EI}{Gct}}\right] \\ C_4 &= w_L \end{aligned}\right\} \tag{A9}$$

An expression for the load P can be obtained from the substitution of equations (A6) and (A9) in equation (A3), as follows:

$$P = \frac{\phi_R\left(\frac{2x}{l} - \frac{2}{3} + \frac{4EI}{Gctl^2}\right) - \phi_L\left(\frac{4}{3} - \frac{2x}{l} + \frac{4EI}{Gctl^2}\right) + 2\left(\frac{2x}{l} - 1\right)\left(\frac{w_R - w_L}{l} + \frac{q_l}{Gt}\right)}{\frac{cl}{EI}\left(\frac{1}{3} + \frac{4EI}{Gctl^2}\right)} \tag{A10}$$

Similarly, from equations (A2), (A6), (A7), and (A9),

$$q_c = \frac{\frac{2}{l}\left(\phi_R + \phi_L\right) + \frac{4}{l^2}\left(w_L - w_R\right) - \frac{cl}{EI}q_l}{\frac{cl}{EI}\left(\frac{1}{3} + \frac{4EI}{Gctl^2}\right)} \tag{A11}$$

The applied loads can now be expressed in terms of the distortions if the foregoing equations are evaluated at the boundaries. These relations for the loads can be conveniently written as follows:

$$P_L = -\alpha\phi_L + \beta\phi_R - (\alpha - \beta)\frac{w_L - w_R}{l} - \delta q_l \tag{A12a}$$

$$P_R = -\beta\phi_L + \alpha\phi_R + (\alpha - \beta)\frac{w_L - w_R}{l} + \delta q_l \tag{A12b}$$

$$q_c = (\alpha - \beta)\frac{\phi_L + \phi_R}{l} + 2(\alpha - \beta)\frac{w_L - w_R}{l^2} - \epsilon q_l \tag{A12c}$$

where

$$\alpha = \frac{1}{\omega}\left(\frac{4}{3} + \frac{4EI}{Gct l^2}\right)$$

$$\beta = \frac{1}{\omega}\left(-\frac{2}{3} + \frac{4EI}{Gct l^2}\right)$$

$$\delta = \frac{1}{\omega}\left(\frac{2}{Gt}\right)$$

$$\epsilon = \frac{1}{\omega}\left(\frac{cl}{3EI}\right)$$

$$\omega = \frac{cl}{EI}\left(\frac{1}{3} + \frac{4EI}{Gct l^2}\right)$$

It is often desirable to express the distortions in terms of the loads. These expressions can be obtained from a few simple operations on equations (A12). Addition of equations (A12a) and (A12b) gives the following relationship between end rotations:

$$\phi_R = \phi_L + \frac{P_L + P_R}{\alpha + \beta}$$

$$= \phi_L + \frac{cl}{2EI}\left(P_L + P_R\right) \tag{A13}$$

Substitution of (A13) into (A12a) or (A12b) yields the following alternate expressions for the difference in end displacements

$$\left.\begin{aligned} w_R - w_L &= \phi_L l + q_l \frac{l}{Gt} + \frac{P_L - P_R}{Gt} + \frac{cl^2}{6EI}\left(2P_L + P_R\right) \\ w_R - w_L &= \phi_R l + q_l \frac{l}{Gt} + \frac{P_L - P_R}{Gt} - \frac{cl^2}{6EI}\left(P_L + 2P_R\right) \end{aligned}\right\} \qquad (A14)$$

APPENDIX B

EFFECTIVE MOMENT OF INERTIA OF BULKHEADS

The contribution of the cover sheets of the box beam to the effective moment of inertia of the bulkheads can be approximated by an analysis of the plate-stringer combination shown in figure 17.

In the analysis the plate and stringer are assumed to be of different materials but of constant cross-sectional dimensions. The contribution of the plate is expressed as an effective width which can be used to determine the area of an equivalent stringer having a total elongation under load the same as that of the stringer in the combined structure. The method of least work (page 156, reference 6) is used to determine the state of stress in the plate and stringer. The stringer stresses can then be integrated over the length of the stringer to determine the total elongation.

The stress distribution in the plate can be defined in terms of a stress function Φ as follows:

$$\left.\begin{aligned} \sigma_x &= \frac{\partial^2 \Phi}{\partial y^2} \\ \sigma_y &= \frac{\partial^2 \Phi}{\partial x^2} \\ \tau_{xy} &= -\frac{\partial^2 \Phi}{\partial x \, \partial y} \end{aligned}\right\} \tag{B1}$$

The stresses given by equations (B1) automatically satisfy equilibrium conditions; the differential equation which the stress function must satisfy to fulfill compatibility is

$$\frac{\partial^4 \Phi}{\partial x^4} + 2\frac{\partial^4 \Phi}{\partial x^2 \partial y^2} + \frac{\partial^4 \Phi}{\partial y^4} = 0 \tag{B2}$$

A solution of equation (B2) is given by

$$\Phi = \sum_{n=1}^{\infty} \left[B_n + C_n\left(1 + \frac{n\pi y}{l}\right) \right] e^{-\frac{n\pi y}{l}} \sin \frac{n\pi x}{l} \tag{B3}$$

In this expression B_n and C_n are arbitrary constants which are determined from the condition that the true stress distribution is that which makes the strain energy of the combined structure a minimum. If the plate width is assumed infinite, the stress function given by equation (B3) satisfies the boundary conditions that all stresses vanish at $y = \infty$ and that $\sigma_x = 0$ when $x = 0$ or l. The stress function does not provide zero shear stress along the edges $x = 0$ and l; therefore, in effect the plate has ribs along these edges. This violation of boundary conditions is considered unimportant since, in the actual structure, these edges are restrained by the spar flanges. The strain energy in the plate is given by the expression

$$U_p = 2\int_0^\infty \int_0^l \frac{t}{2E_p}\left[\sigma_x^2 + \sigma_y^2 - 2\mu\sigma_x\sigma_y + 2(1 + \mu)\tau_{xy}^2\right] dy\, dx \tag{B4}$$

Making substitutions from equations (B1) and (B3) and integrating this expression gives

$$U_p = \frac{\pi^3 t}{l^2}\sum_{n=1}^{\infty} n^3\left(\frac{B_n^2}{2G_p} + \frac{B_n C_n}{2G_p} + \frac{C_n^2}{E_p}\right) \tag{B5}$$

since

$$G_p = \frac{E_p}{2(1 + \mu)}$$

Consideration of equilibrium of plate and stringer gives the following expression for the load in the stringer

$$P_s = P_o - (P_o - P_l)\frac{x}{l} - 2t\int_0^\infty \sigma_x\, dy \tag{B6}$$

The strain energy in the stringer can be written as

$$U_s = \int_0^l \frac{P_s^2}{2AE_s}\, dx \tag{B7}$$

which, upon substitution from equation (B6) and integration, becomes

$$U_s = \frac{l}{6AE_s}\left(P_o^2 + P_o P_l + P_l^2\right) + \frac{\pi^2 t^2}{AE_s l}\sum_{n=1}^{\infty} n^2 B_n^2 + \frac{2t}{AE_s}\sum_{n=1}^{\infty}\left[(-1)^n P_l - P_o\right] B_n \tag{B8}$$

The total strain energy of the system is then

$$U = U_p + U_s \tag{B9}$$

If the total strain energy (equation (B9)) is minimized with respect to B_n and C_n, two equations are obtained which yield the following expressions for the constants

$$B_n = \frac{4l^2\left[P_o - (-1)^n P_l\right]}{A\pi^3 n^2(1 + \mu)(3 - \mu)\left[n\frac{E_s}{E_p} + \frac{4lt}{A\pi(1 + \mu)(3 - \mu)}\right]} \tag{B10a}$$

$$C_n = -B_n\left(\frac{E}{4G}\right)_p$$

$$= -B_n\left(\frac{1 + \mu}{2}\right) \tag{B10b}$$

The total extension of the stringer can now be determined as

$$u = \int_0^l \frac{P_s}{AE_s}\,dx$$

$$= \frac{l}{2AE_s}(P_o + P_l) - \frac{2t}{AE_s}\sum_{n=1}^{\infty}\left[1 - (-1)^n\right]B_n \tag{B11}$$

The effective area of the equivalent stringer is defined as

$$A_e = A + \lambda t_e \tag{B12}$$

where

$$t_e = t\frac{E_p}{E_s}$$

The elongation of the equivalent stringer is then

$$u = \int_0^l \frac{P_s}{A_e E_s}\,dx$$

$$= \frac{l}{2E_s}\left(\frac{P_o + P_l}{A + \lambda t_e}\right) \tag{B13}$$

Setting equation (B11) equal to equation (B13) gives the following equation for the effective width

$$\frac{\lambda}{l} = \left(\frac{A}{lt_e}\right)\frac{N}{\left(\frac{A}{lt_e}\right)\left[\frac{\pi 3(1+\mu)(3-\mu)}{32}\right] - N} \tag{B14}$$

where

$$N = \sum_{n=1,3,5}^{\infty} \frac{1}{n^2\left[n + \left(\frac{lt_e}{A}\right)\frac{4}{\pi(1+\mu)(3-\mu)}\right]}$$

Note that the applied loads do not appear in the expression for effective width.

A similar result can be obtained from an analysis in which the plate is assumed to be infinitely stiff in the transverse (y) direction. In that case, the differential equation of the plate is

$$\frac{\partial^2 u}{\partial x^2} + \left(\frac{G}{E}\right)_p \frac{\partial^2 u}{\partial y^2} = 0 \tag{B15}$$

The solution of equation (B15) which satisfies all the boundary conditions for a plate of width h is

$$u = \sum_{n=1}^{\infty} D_n \frac{\cosh\sqrt{\left(\frac{E}{G}\right)_p}\,\frac{n\pi}{l}(h-y)}{\cosh\sqrt{\left(\frac{E}{G}\right)_p}\,\frac{n\pi h}{l}} \sin\frac{n\pi x}{l} \tag{B16}$$

With the stresses defined in terms of u displacements as follows

$$\sigma_x = E_p \frac{\partial u}{\partial x}$$

$$\tau_{xy} = G_p \frac{\partial u}{\partial y} \tag{B17}$$

and the strain energy of the plate given by

$$U_p = 2\int_0^h \int_0^l \frac{t}{2}\left(\frac{\sigma_x^2}{E_p} + \frac{\tau_{xy}^2}{G_p}\right)dy\,dx \tag{B18}$$

The procedure previously followed can be used to obtain

$$\frac{\lambda}{l} = \left(\frac{A}{lt_e}\right)\frac{N'}{\left(\frac{A}{lt_e}\right)\frac{\pi^3}{8}\sqrt{\frac{1+\mu}{2}} - N'} \tag{B19}$$

where

$$N' = \sum_{n=1,3,5}^{\infty} \frac{\tanh\sqrt{\left(\frac{E}{G}\right)_p}\,\frac{n\pi h}{l}}{n^2\left[n + \left(\frac{lt_e}{A}\right)\frac{1}{\pi}\sqrt{\frac{2}{1+\mu}}\tanh\sqrt{\left(\frac{E}{G}\right)_p}\,\frac{n\pi h}{l}\right]}$$

Examination of equation (B19) reveals that the effect of finite plate width h is negligible whenever $h \geq l$ since the hyperbolic tangent terms very nearly approach a value of 1. In this case only a small difference is found between equations (B14) and (B19).

The two expressions for effective width (equations (B14) and (B19)) have been evaluated for a range of values of A/lt_e when $\mu = \frac{1}{3}$ and $h = \infty$. The results are plotted in figure 18.

The results of the preceding analysis can be presented in a more convenient form for the analysis of a swept wing. The moment of inertia of the bulkhead alone can be related to the area of a substitute stringer as follows:

$$I = \frac{1}{2}Ac^2 \tag{B20}$$

and the effective moment of inertia is

$$I_e = I + \frac{1}{2}\lambda t_e c^2$$

$$= I(1 + \nu) \tag{B21}$$

where

$$\nu = \left(\frac{\lambda}{l}\right)\left(\frac{l t_e}{A}\right)$$

$$= \frac{1}{2}\left(\frac{\lambda}{l}\right)\left(\frac{c^2 l t_e}{I}\right)$$

Figure 8 is a plot of ν as a function of $c^2 l t_e/I$, the results of equation (B14) being used in the solution.

APPENDIX C

NUMERICAL EXAMPLE

Description of Specimen

The application of the method to an actual structure is illustrated by an analysis of the untapered, 45° swept box beam of references 1 and 2. Its construction details and principal dimensions are shown in figure 9. The outer and carry-through sections are of doubly-symmetrical cross section and are divided into five and three bays, respectively, by internal bulkheads placed perpendicular to the spars. It is important to note that the actual structure contains a short bulkhead (bulkhead 7) within the triangular section and that its presence is ignored in the analysis because the method of analysis assumes a triangular section with no internal bulkheads. Figure 10 is a photograph of the specimen under test and illustrates the manner in which it was supported at the four corners of the carry-through section. In the analysis which follows these supports are assumed to be rigid.

The dimensions of the three sections of the idealized structure are summarized in table II and illustrated in figures 19 and 20. The dimensions of the two bulkheads and that portion of the front spar bordering the triangular section are given in table III together with their calculated stiffness factors. The material of the specimen was 24S-T3 aluminum alloy except for the steel bulkheads. These materials are assumed to possess the following elastic properties:

Material	E (psi)	G (psi)
24S-T3	10.5×10^6	4.0×10^6
Steel	29.0×10^6	11.0×10^6

Loading Conditions

The box beam is analyzed under four different loading conditions, symmetrical and antisymmetrical bending and torsion corresponding to the test data of references 1 and 2. These loads are applied to the loading bulkhead at the tip of the outer section; the bending being produced by a vertical shearing force of 2,500 pounds; the torsion by a

pure couple of 43,420 inch-pounds. For convenience, these loadings are hereinafter referred to by number as follows:

Loading 1: Symmetrical tip bending load of 2500 pounds

Loading 2: Antisymmetrical tip bending load of 2500 pounds

Loading 3: Symmetrical tip torque load of 43,420 inch-pounds

Loading 4: Antisymmetrical tip torque load of 43,420 inch-pounds

Analysis of the Outer Section

Method of analysis.- The dimensions of the idealized outer section are given in table II and illustrated in figure 19 which also shows the notation that will be employed. The stress and distortion distributions for the idealized structure will be determined as well as the stiffness factors required for the analysis of the complete structure.

Since the outer section is a cantilever box beam on a flexible root, the stresses and distortions can be obtained from the superposition of the following solutions:

(a) Outer section with a rigid root and a tip bending load of 2500 pounds

(b) Outer section with a rigid root and a tip torque load of 43,420 inch-pounds

(c) Outer section with the root warped

(d) Outer section displaced as a rigid body

A simplification of the analysis and the use of elementary theory in some instances are possible because of the constant doubly-symmetrical cross section. Further simplification is made by assuming that all bulkheads are rigid in their own plane, although this assumption leads to a slight violation of continuity because bulkhead 6 is assumed flexible in the analysis of the triangular section. Figure 21 shows the two types of force groups which appear in this analysis. Shear flows are shown in addition to the concentrated flange forces. The sign convention used with the warping group is that of reference 7.

Bending of a cantilever.- The outer section is considered to be rigidly built in at the root and loaded by a central vertical shearing force of 2500 pounds at the tip as shown in figure 22(a). The internal forces and stresses are those of the F-group and can be expressed as follows:

$$F = \frac{M}{2c} = \frac{V}{2c}(L - x) = 178.57(89 - x) \tag{C1}$$

$$\sigma^B = \sigma^F = \frac{Mc}{2I} = \frac{Vc}{2I}(L - x) = 97.01(89 - x) \tag{C2}$$

$$q_c{}^B = q_c{}^F = \frac{V}{2c} = 178.57 \text{ pounds per inch} \tag{C3}$$

$$\tau_c{}^B = \tau_c{}^F = \frac{q_c{}^B}{t_c} = 2289 \text{ psi} \tag{C4}$$

The beam bends without twisting and the deflection of the center line consists of two components, that due to flexure and that due to shear deformation of the webs. Thus,

$$w^B = w^\sigma + w^\tau \tag{C5}$$

where

$$w^\sigma = \frac{V}{6EI}(3L - x)x^2 = 0.43994(267 - x)x^2 \tag{C6}$$

$$w^\tau = \frac{V}{2Gct_c}x = 0.0005723x \tag{C7}$$

The distribution of stress and deflection is given in table IV(a).

Torsion of a cantilever.- The outer section is considered to be rigidly built in at the root and loaded by a pure couple of 43,420 inch-pounds at the tip as shown in figure 22(b). The internal forces and stresses are those of the X-group plus the shear stresses required to equilibrate the torque and can be expressed as follows:

$$\sigma_n{}^T = \frac{X_n{}^T}{A} \tag{C8}$$

$$(\tau t)_{c,n}{}^T = q_{c,n}{}^T = \frac{T_n}{2bc} + q_{c,n}{}^X = \frac{T_n}{2bc} + \frac{X_n{}^T - X_{n-1}{}^T}{2a_n} \tag{C9}$$

$$(\tau t)_{b,n}{}^{T} = q_{b,n}{}^{T} = \frac{T_n}{2bc} + q_{b,n}{}^{X} = \frac{T_n}{2bc} - \frac{X_n{}^{T} - X_{n-1}{}^{T}}{2a_n} \qquad (C10)$$

The X-forces are statically indeterminate; however, they can be calculated by means of the following recurrence relation (reference 7) which establishes continuity between bays:

$$f_n X_{n-1}{}^{T} - \left(p_n + p_{n+1}\right) X_n{}^{T} + f_{n+1} X_{n+1}{}^{T} = -j_n T_n + j_{n+1} T_{n+1} \qquad (C11)$$

where

$$p = \frac{a}{3AE} + \frac{1}{8Ga}\left(\frac{b}{t_b} + \frac{c}{t_c}\right)$$

$$f = -\frac{a}{6AE} + \frac{1}{8Ga}\left(\frac{b}{t_b} + \frac{c}{t_c}\right)$$

$$j = \frac{1}{8Gbc}\left(\frac{b}{t_b} - \frac{c}{t_c}\right)$$

in which A is the effective area for warping stress.

Once the X-forces are known, the twist of one bulkhead relative to the next can be determined as follows (reference 8):

$$\Delta\theta_n{}^{T} = \left(\frac{Ta}{GJ}\right)_n + \Delta\theta_n{}^{X}$$

$$= \left(\frac{Ta}{GJ}\right)_n - 4j_n\left(X_n{}^{T} - X_{n-1}{}^{T}\right) \qquad (C12)$$

where

$$J = \frac{2b^2c^2}{\frac{b}{t_b} + \frac{c}{t_c}}$$

For the dimensions and stiffness parameters given in table II, the recurrence relation yields the following set of simultaneous equations for the X-forces:

$$\begin{bmatrix} -3.57806 & 0.57511 & 0 & 0 & 0 \\ 0.57511 & -3.57806 & 0.57511 & 0 & 0 \\ 0 & 0.57511 & -4.15317 & 1.75718 & 0 \\ 0 & 0 & 1.75718 & -4.72828 & 1.75718 \\ 0 & 0 & 0 & 1.75718 & -2.36414 \end{bmatrix} \begin{bmatrix} X_2{}^T \\ X_3{}^T \\ X_4{}^T \\ X_5{}^T \\ X_6{}^T \end{bmatrix} = \begin{bmatrix} 0 \\ 0 \\ 0 \\ 0 \\ 3296.924 \end{bmatrix}$$

The solutions are

$$X_2{}^T = -10.573$$
$$X_3{}^T = -65.779$$
$$X_4{}^T = -398.673$$
$$X_5{}^T = -920.751$$
$$X_6{}^T = -2078.917$$

The distribution of stress and twist is given in table IV(b).

Warping of the root.- The root of the outer section is warped the amount shown in figure 22(c). The internal forces and stresses are those of the X-group which can be determined by the method of analysis used in the preceding section. The only change is in the boundary conditions with the warping of the root being related to the X-forces as follows:

$$f_6 X_5{}^W - p_6 X_6{}^W = \frac{c}{4}\left(\phi_2 - \phi_3\right) \qquad (C13)$$

The solutions of the system of equations are then

$$X_2{}^W = -5612\left(\phi_2 - \phi_3\right)$$
$$X_3{}^W = -34915\left(\phi_2 - \phi_3\right)$$
$$X_4{}^W = -211615\left(\phi_2 - \phi_3\right)$$

$$X_5^W = -488733(\phi_2 - \phi_3)$$

$$X_6^W = -1103484(\phi_2 - \phi_3)$$

Table IV(c) summarizes the stress and twist distributions for $(\phi_2 - \phi_3) = 1 \times 10^{-6}$.

Rigid-body displacements.- The outer section is given the rigid-body displacements shown in figures 22(d) and 22(e). These displacements do not affect the stress distribution but give the outer section a twist about its center line

$$\theta^R = \frac{w_2}{b} \tag{C14}$$

plus a deflection of that center line

$$w^R = \frac{1}{2}w_2 + \frac{1}{2}(\phi_2 + \phi_3)x \tag{C15}$$

Superposition of solutions.- The complete stress and distortion distributions can be obtained by combining components from each of the preceding analyses. Since the basic expressions are the same for both symmetrical and antisymmetrical loads, the stresses and distortions at any cross section can be written as follows:

	Loadings 1 and 2	Loadings 3 and 4
σ_F	$\sigma^B + \sigma^W$	$\sigma^T + \sigma^W$
σ_R	$\sigma^B - \sigma^W$	$-\sigma^T - \sigma^W$
τ_f	$-\tau_c^B - \tau_c^W$	$-\tau_c^T - \tau_c^W$
τ_r	$\tau_c^B - \tau_c^W$	$-\tau_c^T - \tau_c^W$
τ_b	$-\tau_b^W$	$-\tau_b^T - \tau_b^W$
θ	$\theta^R + \theta^W$	$\theta^R + \theta^T + \theta^W$
w	$w^R + w^B$	w^R

(C16)

The sign convention for the stresses is that shown for the internal

forces of the outer section in figure 2. Positive deflections and twist move the front spar downward. Similar expressions can be written for the forces at the root cross section from which the stiffness factors given in table V can be determined by inspection. These are the stiffness factors required for the analysis of the complete structure.

Analysis of the Carry-Through Section

Method of analysis.- The dimensions of the idealized carry-through section are given in table II and illustrated in figure 20, which also shows the notation employed. The stress distribution is determined along with the stiffness factors required for the analysis of the complete structure.

Since the supports at the four corners of the carry-through section are assumed to be rigid $(w_1 = w_3 = 0)$, the stiffness factors associated with the deflection and twist of the ends in the plane of the end cross sections will not be required. The stresses can therefore be obtained from the superposition of the following solutions:

(a) Carry-through section with the end cross sections rotated out of their original planes

(b) Carry-through section with the end cross sections warped out of their original planes

The doubly-symmetrical cross section permits considerable simplification of the analysis since in such cases the end rotation is a result of the application of F-forces only and the warping is the result of the application of X-forces only (fig. 21); however, a few complications are introduced because the splices in the center bay make it stiffer than the other two bays. The bulkheads are assumed rigid in their own plane despite the fact that in the analysis of the adjacent triangular section, bulkhead 8 is assumed to be flexible.

Since the analysis depends upon whether the end distortions are symmetrical or antisymmetrical, the ratio R is introduced in order that general equations, applicable to both types of loading, can be written. Then:

R = +1 when the loading is symmetrical

R = -1 when the loading is antisymmetrical

Rotation of the ends.- The ends of the carry-through section are rotated, symmetrically or antisymmetrically by the amount shown in figure 23(a). Equilibrium of internal forces requires that:

$$q_{c,9}{}^{F} = q_{c,10}{}^{F} = \frac{F_{10} - F_9}{a_{10}} = \frac{F_9 - F_8}{a_9} \tag{C17}$$

The forces can now be related to the distortions by means of equations (A13) and (A14) as follows:

$$\phi_9 = \phi_8 - 2\left(\frac{ca}{2EI}\right)\left(F_8 + F_9\right) \tag{C18}$$

$$w_9 - w_{10} = \phi_9 a_{10} - 2\frac{F_9 - F_{10}}{(2Gt_c)_{10}} - 2\left(\frac{ca^2}{6EI}\right)_{10}\left(2F_8 + F_{10}\right) \tag{C19}$$

$$w_8 - w_9 = \phi_9 a_9 - 2\frac{F_8 - F_9}{(2Gt_c)_9} + 2\left(\frac{ca^2}{6EI}\right)_9\left(F_8 + 2F_9\right) \tag{C20}$$

and since

$$w_8 = w_{11} = 0 \tag{C21}$$

$$R = \frac{F_{10}}{F_9} = \frac{F_{11}}{F_8} = \frac{w_{10}}{w_9} = -\frac{\phi_{10}}{\phi_9} = -\frac{\phi_{11}}{\phi_8} \tag{C22}$$

$$\phi_8 = \frac{1}{2}\left(\psi_1 + \psi_3 \sin\Lambda + \phi_3 \cos\Lambda\right) \tag{C23}$$

the following relationships can be obtained:

$$F_8 = \frac{\frac{1}{2}\left[a_{10} + (1 - R)a_9\right]^2\left(\psi_1 + \psi_3 \sin\Lambda + \phi_3 \cos\Lambda\right)}{\frac{1 - R}{G}\left[\left(\frac{a}{t_c}\right)_{10} + (1 - R)\left(\frac{a}{t_c}\right)_9\right] + \left(\frac{ca}{EI}\right)_{10}\frac{(2 + R)a_{10}{}^2}{3} + 2\left(\frac{ca}{EI}\right)_9\left[a_{10}{}^2 + (1 - R)a_{10}a_9 + \frac{(1 - R)^2}{3}a_9{}^2\right]} \tag{C24}$$

$$F_9 = F_8 \frac{1}{1 + \frac{a_9}{a_{10}}(1 - R)} \tag{C25}$$

$$q_{c,9}^{F} = q_{c,10}^{F} = F_8 \frac{1 - R}{a_{10} + (1 - R)a_9} \tag{C26}$$

The stress distribution corresponding to end rotations of the amount $\psi_1 + \psi_3 \sin \Lambda + \psi_3 \cos \Lambda = 1 \times 10^{-6}$ is given in table VI(a), in which

$$\sigma_n^{B} = \left(\frac{Fc^2}{I}\right)_n \tag{C27}$$

$$\tau_{c,n}^{B} = \left(\frac{q_c^{F}}{t_c}\right)_n \tag{C28}$$

Warping of the ends.- The ends of the carry-through section are warped, symmetrically or antisymmetrically, by the amount shown in figure 23(b). Then, since

$$R = \frac{X_{10}}{X_9} = \frac{X_{11}}{X_8} = -\frac{\psi_{10}}{\psi_9} = -\frac{\psi_{11}}{\psi_8} \tag{C29}$$

and

$$\psi_8 = \frac{1}{2}\left(\psi_1 - \psi_3 \sin \Lambda - \phi_3 \cos \Lambda\right) \tag{C30}$$

the method of reference 7 can be used to obtain the following equations for the warping forces:

$$p_9 X_8 - f_9 X_9 + j_9 T = \frac{c}{4}\left(\psi_1 - \psi_3 \sin \Lambda - \phi_3 \cos \Lambda\right) \tag{C31}$$

$$-f_9 X_8 + \left(p_9 + p_{10} - R f_{10}\right) X_9 + \left(j_{10} - j_9\right) T = 0 \tag{C32}$$

The torque in the carry-through section is statically indeterminate for antisymmetrical loadings but can be determined from the condition that one end does not twist relative to the other because of the rigid supports, that is:

$$\Delta\theta_9 + \Delta\theta_{10} + \Delta\theta_{11} = 0 \tag{C33}$$

which can be written as follows by use of the equations of reference 8:

$$4(1 - R)j_9X_8 - 4(1 - R)(j_9 - j_{10})X_9 + \left[2\left(\frac{a}{GJ}\right)_9 + \left(\frac{a}{GJ}\right)_{10}\right]_T = 0 \qquad (C34)$$

The stiffness parameters f, j, p, and $\frac{a}{GJ}$ have been previously defined in the section "Analysis of the Outer Section" of this appendix and their numerical values for the carry-through section are listed in table II. These values can be used to obtain the following sets of simultaneous equations and solutions:

Symmetrical loads:

$$\begin{bmatrix} 3.349163 & -2.874949 & 0.0797693 \\ -2.874949 & 3.727325 & -.0388418 \\ 0 & 0 & .0336914 \end{bmatrix} \begin{bmatrix} X_8 \\ X_9 \\ T \end{bmatrix} = \begin{bmatrix} 1.75(\psi_1 - \psi_3 \sin\Lambda - \phi_3 \cos\Lambda) \\ 0 \\ 0 \end{bmatrix}$$

$$X_8 = 1546392(\psi_1 - \psi_3 \sin\Lambda - \phi_3 \cos\Lambda)$$

$$X_9 = 1192759(\psi_1 - \psi_3 \sin\Lambda - \phi_3 \cos\Lambda)$$

$$T = 0$$

Antisymmetrical loads:

$$\begin{bmatrix} 3.349163 & -2.874949 & 0.0797693 \\ -2.874949 & 7.096181 & -.0388418 \\ .638154 & -.310734 & .0336914 \end{bmatrix} \begin{bmatrix} X_8 \\ X_9 \\ T \end{bmatrix} = \begin{bmatrix} 1.75(\psi_1 - \psi_3 \sin\Lambda - \phi_3 \cos\Lambda) \\ 0 \\ 0 \end{bmatrix}$$

$$X_8 = 1509857(\psi_1 - \psi_3 \sin\Lambda - \phi_3 \cos\Lambda)$$

$$X_9 = 479367(\psi_1 - \psi_3 \sin\Lambda - \phi_3 \cos\Lambda)$$

$$T = -24177260(\psi_1 - \psi_3 \sin\Lambda - \phi_3 \cos\Lambda)$$

The stress distribution corresponding to end warpings of $(\psi_1 - \psi_3 \sin\Lambda - \phi_3 \cos\Lambda) = 1 \times 10^{-6}$ is given in table VI(b), in which

$$\sigma_n^W = \left(\frac{X}{A}\right)_n \tag{C35}$$

$$\tau_{c,n}^W = \frac{1}{t_{c,n}}\left(\frac{T_n}{2bc} + \frac{X_n - X_{n-1}}{2a_n}\right) \tag{C36}$$

$$\tau_{b,n}^W = \frac{1}{t_{b,n}}\left(\frac{T_n}{2bc} - \frac{X_n - X_{n-1}}{2a_n}\right) \tag{C37}$$

Superposition of solutions.- The complete stress distribution can be obtained by combining the components from each of the preceding analyses. The basic expressions are the same for all types of loading; thus, the stresses on any cross section can be written as follows:

$$\left.\begin{aligned} \sigma_F &= \sigma^B + \sigma^W \\ \sigma_R &= \sigma^B - \sigma^W \\ \tau_f &= -\tau_c^B - \tau_c^W \\ \tau_r &= \tau_c^B - \tau_c^W \\ \tau_b &= -\tau_b^W \end{aligned}\right\} \tag{C38}$$

The sign convention for the stresses is that shown for the internal forces of the carry-through section in figure 2. Similar expressions can be written for the end forces from which the stiffness factors given in table VII can be determined by inspection. These are the stiffness factors required for the analysis of the complete structure.

Stiffness Factors of the Beams

The dimensions and stiffness factors of the two bulkheads and the portion of the front spar which bound the triangular section are given in table III.

Since the nature of the normal-stress distribution in the triangular-section cover influences the effective moment of inertia of the front spar, two values are given. They were determined as follows:

For bending stresses, I_e was taken as one-half the moment of inertia of the doubly-symmetrical outer section.

For warping stresses, I_e was determined from the effective warping area of the outer section; thus,

$$I_e = \frac{1}{2}Ac^2 = \frac{1}{2}(0.863)(7)^2 = 21.1 \text{ inches}^4 \qquad (C39)$$

The effective moment of inertia of the bulkheads includes a contribution from the cover sheet of the box beam as determined from figure 8. The equivalent thickness of the aluminum-alloy sheet acting with the steel bulkhead is given by the relationship

$$t_e = t\frac{E_{sheet}}{E_{bulkhead}} = 0.050\left(\frac{10.5}{29.0}\right) = 0.0181 \text{ inches} \qquad (C40)$$

Triangular Cover Sheet

The shear stiffness of the triangular cover sheet, which frequently appears in the general equations, has the following value:

$$\frac{Gtc}{2} = \frac{1}{2}(4 \times 10^6)(0.050)(7) = 700{,}000 \text{ pounds} \qquad (C41)$$

The shear stiffness per unit width also appears and is

$$\frac{Gtc}{2b} = \frac{1}{30}(700{,}000) = 23{,}333 \text{ pounds per inch} \qquad (C42)$$

The Systems of Equations and Their Solutions

Sufficient data have now been obtained to permit evaluation of the coefficients of the matrix (table I); however, since the supports have been assumed rigid ($w_1 = w_3 = 0$), it will be unnecessary to evaluate the coefficients of w_1/b and w_3/b. Furthermore, there are only seven unknown joint displacements, which require only seven equations. The logical equations to eliminate are equations (3) and (9) since they contain the support reactions V_1 and V_3, which are statically indeterminate for the antisymmetrical loading conditions. The joint force V_2 is zero because the loads are applied at the tips only.

A different set of equations will be required for each loading condition since the structure responds differently in each case. Thus, the stiffness factors for the carry-through section are different for symmetrical and antisymmetrical loads and the effective moment of inertia of the front spar and the loading terms are different for bending and torsion. The calculated coefficients are given in matrix form in

table VIII. Each block in the table has space for four values, one for each loading condition. If a single values is given, that coefficient is good for all four loading conditions; when two values are listed, the upper one is for loadings 1 and 2 whereas the lower one is for loadings 3 and 4; and if four values appear, they are for loadings 1, 2, 3, and 4, respectively, when reading from top to bottom.

Throughout the calculations, a large number of significant figures have been carried, more than are justified by the accuracy of the initial data; however, the extra figures were carried in order to obtain an accurate check on the numerical work when the calculated internal forces are substituted into the original nine equilibrium equations. The solution of the equations and the calculation of internal forces frequently involve the differences of large numbers and the final results are apt to contain several significant figures less than the initial coefficients.

The solution of the systems of equations yields the joint displacements given in table IX. Many methods are available for the solution of simultaneous linear equations; however, the method of reference 9 is recommended because of its many practical advantages.

Calculation of Stresses

The flange forces and shear flows in and around the triangular section can be obtained from the joint displacements by substituting them back into the force-displacement relationships, equations (13) to (35). The shear stress is given by the shear flow divided by the sheet thickness; thus,

$$\tau = \frac{q}{t} \tag{C43}$$

The flange stress in the front spar and bulkheads is obtained from the flange force and the effective moment of inertia as follows:

$$\sigma = \frac{Pc^2}{2I_e} \tag{C44}$$

The flange stresses in the outer and carry-through sections must be determined by summing up the various component stresses, equations (C16) and (C38), since different effective areas are associated with the bending and warping stresses. The results of these calculations are given in table X.

The stress distribution in the outer and carry-through sections can be obtained as described in the analysis of these sections, with joint

displacements substituted where necessary. The results are given in tables XI and XII, respectively.

Figure 12 illustrates the distribution of flange normal stresses and spar shear stresses as calculated in this example and compares them with the experimental data of references 1 and 2. The distribution of normal stress in the cover at three selected stations is similarly illustrated in figure 13.

Calculation of Distortions

The distortions of the outer section can be calculated by adding up a number of component distortions as provided in equations (C16). The deflections of the individual spars can be obtained from the deflection and twist of the box beam as follows:

$$w_F = w + \frac{1}{2}\theta b$$

$$w_R = w - \frac{1}{2}\theta b \qquad (C45)$$

The twist of the structure in a plane parallel to the flight path contains a component of the twist perpendicular to the spars and a component of the rate of change of deflection, but it is most easily calculated from the deflections of the individual spars.

The calculated results are listed in table XIII and are graphically compared with the experimental data of references 1 and 2 in figure 11.

REFERENCES

1. Zender, George, and Libove, Charles: Stress and Distortion Measurements in a 45° Swept Box Beam Subjected to Bending and to Torsion. NACA TN 1525, 1948.

2. Zender, George W., and Heldenfels, Richard R.: Stress and Distortion Measurements in a 45° Swept Box Beam Subjected to Antisymmetrical Bending and Torsion. NACA TN 2054, 1950.

3. Levy, Samuel: Computation of Influence Coefficients for Aircraft Structures with Discontinuities and Sweepback. Jour. Aero. Sci. vol. 14, no. 10, Oct. 1947, pp. 547-560.

4. Kuhn, Paul: A Procedure for the Shear-Lag Analysis of Box Beams. NACA ARR, Jan. 1943.

5. Kuhn, Paul: Stress Analysis of Beams with Shear Deformation of the Flanges. NACA Rep. 608, 1937.

6. Timoshenko, S.: Theory of Elasticity. First ed., McGraw-Hill Book Co., Inc., 1934.

7. Kuhn, Paul: A Method of Calculating Bending Stresses Due to Torsion. NACA ARR, Dec. 1942.

8. Kuhn, Paul: Deformation Analysis of Wing Structures. NACA TN 1361, 1947.

9. Crout, Prescott D.: A Short Method for Evaluating Determinants and Solving Systems of Linear Equations with Real or Complex Coefficients. Trans. AIEE, vol. 60, 1941, pp. 1235-1240. (Abridged as Marchant Methods MM-182, Sept. 1941, Marchant Calculating Machine Co., Oakland, Calif.)

TABLE I.- COEFFICIENTS (a_{ij}) OF THE GENERAL MATRIX DEFINING THE JOINT DISPLACEMENTS

Coefficient	Formula
a_{11}	$\left[\left(k_{15} + k_{16}\right) - \left(k_{11} + k_{12}\right)\right] \sec \Lambda + (\alpha + \beta)_{12} \cos \Lambda$
a_{21}	$-(\alpha + \beta)_{12} \cos \Lambda$
a_{31}	$\left(k_{19} + k_{20}\right) - \left(k_{27} + k_{28}\right)$
a_{41}	$-\beta_{12} \cos \Lambda - \frac{Gtc}{2b} \delta_{12} \cos \Lambda$
a_{51}	$-\frac{Gtc}{2b} \cos \Lambda$
a_{61}	$(\alpha - \beta)_{12} \cos \Lambda + \frac{Gtc}{2} \left(\epsilon_{12} + \epsilon_{23}\right) \sin \Lambda$
a_{71}	$\left(k_{23} + k_{24}\right)\delta_{13} \sec \Lambda - \frac{Gtc}{2b} \delta_{13} \cos 2\Lambda$
a_{81}	$\left(k_{11} + k_{12}\right) \sec \Lambda + \frac{Gtc}{2} \sin \Lambda$
a_{91}	$-\left[\epsilon_{13}\left(k_{23} + k_{24}\right) + \left(k_{27} + k_{28}\right)\right] b \sec \Lambda + \frac{Gtc}{2}\left(\epsilon_{13} \cos 2\Lambda - \epsilon_{23}\right)$
a_{12}	$(\alpha + \beta)_{23} \tan \Lambda$
a_{22}	$(\alpha + \beta)_{23} \cot \Lambda$
a_{32}	0
a_{42}	$\frac{Gtc}{2b} \delta_{12} \cot \Lambda$
a_{52}	$\frac{\alpha_{23}}{\delta_{23}} + \frac{Gtc}{2b} \cot \Lambda$
a_{62}	$(\alpha - \beta)_{23} \tan \Lambda - \frac{Gtc}{2}\left(\epsilon_{12} + \epsilon_{23}\right)$
a_{72}	$(\alpha + \beta)_{23} + \frac{Gtc}{2b} \delta_{13} \cos 2\Lambda \csc \Lambda$
a_{82}	$-(\alpha + \beta)_{23} \tan \Lambda - \frac{Gtc}{2}$
a_{92}	$-(\alpha - \beta)_{23} \sec \Lambda - \frac{Gtc}{2}\left(\epsilon_{13} \cos 2\Lambda - \epsilon_{23}\right) \csc \Lambda$

TABLE I.- COEFFICIENTS (a_{ij}) OF THE GENERAL MATRIX DEFINING THE JOINT DISPLACEMENTS - Continued

Coefficient	Formula
a_{13}	$\left[\left(k_{15} - k_{16}\right) - \left(k_{11} - k_{12}\right)\right] \tan \Lambda - (\alpha + \beta)_{23} \tan \Lambda$
a_{23}	$-(\alpha + \beta)_{13} \cot \Lambda - (\alpha + \beta)_{23} \cot \Lambda$
a_{33}	$\left[\left(k_{19} - k_{20}\right) - \left(k_{27} - k_{28}\right)\right] \sin \Lambda$
a_{43}	0
a_{53}	$-\frac{\beta_{23}}{\delta_{23}}$
a_{63}	$(\alpha - \beta)_{23} \tan \Lambda$
a_{73}	$\left(k_{23} - k_{24}\right)\delta_{13} \tan \Lambda - \alpha_{13} - (\alpha + \beta)_{23}$
a_{83}	$\left(k_{11} - k_{12}\right) \tan \Lambda + (\alpha + \beta)_{23} \tan \Lambda$
a_{93}	$-\left[\epsilon_{13}\left(k_{23} - k_{24}\right) + \left(k_{27} - k_{28}\right)\right] b \tan \Lambda - (\alpha - \beta)_{13} \cos \Lambda - (\alpha - \beta)_{23} \sec \Lambda$
a_{14}	$(\alpha + \beta)_{12} \sin \Lambda$
a_{24}	$-(\alpha + \beta)_{12} \sin \Lambda - (\alpha + \beta)_{13} \csc \Lambda$
a_{34}	0
a_{44}	$-\beta_{12} \sin \Lambda + \frac{Gtc}{2b} \delta_{12} \cos \Lambda \cot \Lambda$
a_{54}	$\frac{Gtc}{2b} \cos \Lambda \cot \Lambda$
a_{64}	$(\alpha - \beta)_{12} \sin \Lambda - \frac{Gtc}{2}\left(\epsilon_{12} + \epsilon_{23}\right) \cos \Lambda$
a_{74}	$-\beta_{13} \sec \Lambda + \frac{Gtc}{2b} \delta_{13} \cos 2\Lambda \cot \Lambda$
a_{84}	$-\frac{Gtc}{2} \cos \Lambda$
a_{94}	$(\alpha - \beta)_{13} - \frac{Gtc}{2}\left(\epsilon_{13} \cos 2\Lambda - \epsilon_{23}\right) \cot \Lambda$

TABLE I.- COEFFICIENTS (a_{ij}) OF THE GENERAL MATRIX DEFINING THE JOINT DISPLACEMENTS - Continued

Coefficient	Formula
a_{15}	$-(\alpha + \beta)_{12}$
a_{25}	$(\alpha + \beta)_{12}$
a_{35}	0
a_{45}	$k_3 + \alpha_{12} + \frac{Gtc}{2b}\delta_{12}$
a_{55}	$-k_7 + \frac{Gtc}{2b}$
a_{65}	$-(1 - \epsilon_{23})k_7 b \tan\Lambda + (\alpha - \beta)_{12} - \frac{Gtc}{2}(\epsilon_{12} + \epsilon_{23}) \tan\Lambda$
a_{75}	$-k_3 \tan\Lambda + \frac{Gtc}{2b}\delta_{13} \cos 2\Lambda \sec\Lambda$
a_{85}	$-k_3 - \frac{Gtc}{2}\tan\Lambda$
a_{95}	$(1 - \epsilon_{23})k_7 b \sec\Lambda - \frac{Gtc}{2}(\epsilon_{13} \cos 2\Lambda - \epsilon_{23}) \sec\Lambda$
a_{16}	$(k_{15} - k_{16}) - (k_{11} - k_{12})$
a_{26}	$(\alpha + \beta)_{13}$
a_{36}	$(k_{19} - k_{20}) \cos\Lambda - (k_{27} - k_{28}) \cos\Lambda$
a_{46}	$-k_3 - \frac{Gtc}{2b}\delta_{12}$
a_{56}	$k_7 - \frac{Gtc}{2b}$
a_{66}	$(1 - \epsilon_{23})k_7 b \tan\Lambda + \frac{Gtc}{2}(\epsilon_{12} + \epsilon_{23}) \tan\Lambda$
a_{76}	$k_3 \tan\Lambda + \delta_{13}(k_{23} - k_{24}) + \alpha_{13} \tan\Lambda - \frac{Gtc}{2b}\delta_{13} \cos 2\Lambda \sec\Lambda$
a_{86}	$k_3 + (k_{11} - k_{12}) + \frac{Gtc}{2}\tan\Lambda$
a_{96}	$-(1 - \epsilon_{23})k_7 b \sec\Lambda - \left[\epsilon_{13}(k_{23} - k_{24}) + (k_{27} - k_{28})\right] b + (\alpha - \beta)_{13} \sin\Lambda + \frac{Gtc}{2}(\epsilon_{13} \cos 2\Lambda - \epsilon_{23}) \sec\Lambda$

TABLE I.- COEFFICIENTS (a_{ij}) OF THE GENERAL MATRIX DEFINING THE JOINT DISPLACEMENTS - Continued

Coefficient	Formula
a_{17}	$\left[\left(k_{17} + k_{18}\right) - \left(k_{13} + k_{14}\right)\right] b \sec \Lambda$
a_{27}	0
a_{37}	$\left[\left(k_{21} + k_{22}\right) - \left(k_{29} + k_{30}\right)\right] b$
a_{47}	$(\alpha - \beta)_{12} \cot \Lambda$
a_{57}	0
a_{67}	$2(\alpha - \beta)_{12} \cot \Lambda$
a_{77}	$\left(k_{25} + k_{26}\right)\delta_{13} b \sec \Lambda + (\alpha - \beta)_{13}$
a_{87}	$\left(k_{13} + k_{14}\right) b \sec \Lambda$
a_{97}	$-\left[\epsilon_{13}\left(k_{25} + k_{26}\right) + \left(k_{29} + k_{30}\right)\right] b^2 \sec \Lambda + 2(\alpha - \beta)_{13} \cos \Lambda$
a_{18}	0
a_{28}	0
a_{38}	0
a_{48}	$-(\alpha - \beta)_{12} \cot \Lambda$
a_{58}	$-(\alpha - \beta)_{23} \frac{1}{\delta_{23}}$
a_{68}	$-2(\alpha - \beta)_{12} \cot \Lambda - 2(\alpha - \beta)_{23} \tan \Lambda$
a_{78}	0
a_{88}	0
a_{98}	$2(\alpha - \beta)_{23} \sec \Lambda$

TABLE I.- COEFFICIENTS (a_{ij}) OF THE GENERAL MATRIX DEFINING THE JOINT DISPLACEMENTS - Concluded.

Coefficient	Formula
a_{19}	$\left[\left(k_{17} - k_{18}\right) - \left(k_{13} - k_{14}\right)\right] b \sec \Lambda$
a_{29}	0
a_{39}	$\left[\left(k_{21} - k_{22}\right) - \left(k_{29} - k_{30}\right)\right] b$
a_{49}	0
a_{59}	$(\alpha - \beta)_{23} \frac{1}{\delta_{23}}$
a_{69}	$2(\alpha - \beta)_{23} \tan \Lambda$
a_{79}	$\left(k_{25} - k_{26}\right)\delta_{13} b \sec \Lambda - (\alpha - \beta)_{13}$
a_{89}	$\left(k_{13} - k_{14}\right) b \sec \Lambda$
a_{99}	$-\left[\epsilon_{13}\left(k_{25} - k_{26}\right) + \left(k_{29} - k_{30}\right)\right] b^2 \sec \Lambda -$ $2(\alpha - \beta)_{13} \cos \Lambda - 2(\alpha - \beta)_{23} \sec \Lambda$
a_{10}	$-\left(k_1 + k_4\right) M$
a_{20}	$\left(k_1 + k_4\right) M$
a_{30}	$-\frac{1}{c}\left(V_1 + V_2 + V_3\right) + \left(k_5 + k_{10}\right) V$
a_{40}	$k_4 M + k_2 T$
a_{50}	$-k_8 V - k_9 T$
a_{60}	$\left[-\frac{1}{c} V_2 + \left(k_5 + \epsilon_{23} k_8\right) V + \left(k_6 + \epsilon_{23} k_9\right) T\right] b \tan \Lambda$
a_{70}	$\left(k_1 M - k_2 T\right) \tan \Lambda$
a_{80}	$k_1 M - k_2 T$
a_{90}	$\left[-\frac{1}{c} V_3 + \left(k_{10} - \epsilon_{23} k_8\right) V - \left(k_6 + \epsilon_{23} k_9\right) T\right] b \sec \Lambda$

TABLE II.- DIMENSIONS AND STIFFNESS PARAMETERS OF IDEALIZED STRUCTURE USED IN THE NUMERICAL EXAMPLE

Item	Outer section (fig. 19)		Triangular section	Carry-through section (fig. 20)	
	Bays 2, 3 and 4	Bays 5 and 6		Bays 9 and 11	Bay 10
Dimensions					
b, in.	30	30	30	-----	-----
b', in.	-----	-----	-----	42.1	42.1
c, in.	7	7	7	7	7
t_b, in.	0.050	0.050	0.050	0.050	*0.0885
t_c, in.	0.078	0.078	0.078	0.078	0.078
a, in.	22	11	30	9.60	9.76
I, in^4	90.2	90.2	-----	122.58	135.15
**A, sq in.	0.863	0.863	-----	0.964	1.229
Stiffness parameters					
***p, in./lb	1.78903×10^{-6}	2.36414×10^{-6}	-----	3.349163×10^{-6}	2.062590×10^{-6}
f, in./lb	0.57511×10^{-6}	1.75718×10^{-6}	-----	2.874949×10^{-6}	1.684428×10^{-6}
j, per lb	0.075931×10^{-6}	0.075931×10^{-6}	-----	0.0797693×10^{-6}	0.0409275×10^{-6}
a/GJ, per in.-lb	0.0430112×10^{-6}	0.0215056×10^{-6}	-----	0.0128741×10^{-6}	0.0079432×10^{-6}

*Includes an allowance for splice plates.

**Effective area for warping stress $\left(A = A_f + \frac{1}{6}ct_c + \frac{1}{6}bt_b + \frac{1}{6}\sum A_s\right)$

***These stiffness parameters are defined in appendix C.

TABLE III.- DIMENSIONS AND STIFFNESS FACTORS OF THE BEAMS

Beam	Front spar 1-2		Bulkhead 2-3	Bulkhead 1-3
Material	24S-T3 aluminum alloy		Steel	Steel
Stress	Bending	Warping		
Dimensions				
l, in.	30	30	29.25	41.34
c, in.	7	7	7	7
t, in.	0.078	0.078	0.125	0.125
I, in.^{4}	-----	-----	6.15	8.01
t_e, in.	-----	-----	0.0181	0.0181
$c^2 l t_e/I$	-----	-----	4.21	4.57
ν	-----	-----	0.60	0.65
I_e, in.^{4}	45.1	21.1	9.84	13.21
Stiffness factors				
ω, per lb	0.575170×10^6	0.743315×10^6	0.338627×10^6	0.332182×10^6
α, lb	3.993615×10^6	2.400311×10^6	4.346797×10^6	4.427535×10^6
β, lb	0.516384×10^6	-0.290336×10^6	-1.559397×10^6	-1.780133×10^6
δ, in.	11.14498	8.623871	4.295415	4.51467
ϵ	0.257002	0.425063	0.706297	0.781584

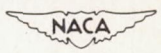

TABLE IV.- STRESS AND DISTORTION DISTRIBUTION IN OUTER SECTION

(a) When root is rigidly built-in and tip bending load of 2500 pounds is applied

n	x (in.)	F^B (lb)	σ^B (psi)	$\tau_c{}^B$ (psi)	w^σ (in.)	w^T (in.)	w^B (in.)
1	88	176	97	-----	0.6098	0.0504	0.6602
2	66	4107	2231	2289	.3852	.0378	.4230
3	44	8036	4365	2289	.1899	.0252	.2151
4	22	11964	6500	2289	.0522	.0126	.0648
5	11	13929	7567	2289	.0136	.0063	.0199
6	0	15893	8634	2289	0	0	0

(b) When root is rigidly built-in and tip torque of 43,420 inch pounds is applied

n	σ^T (psi)	$\tau_c{}^T$ (psi)	$\tau_b{}^T$ (psi)	Ta/GJ (radians)	$\Delta\theta^X$ (radians)	θ^T (radians)
1	0	-----	-----	---------	--------	-0.006840
2	-13	-1328	-2063	-0.001868	0.000003	-.004975
3	-76	-1341	-2043	-.001868	.000017	-.003124
4	-462	-1422	-1916	-.001868	.000101	-.001357
5	-1067	-1630	-1593	-.000934	.000159	-.000582
6	-2409	-2000	-1015	-.000934	.000352	0

(c) When root is warped by amount $(\phi_2 - \phi_3) = 1 \times 10^{-6}$ radians

n	σ^W (psi)	$\tau_c{}^W$ (psi)	$\tau_b{}^W$ (psi)	$\Delta\theta^W$ (radians)	θ^W (radians)
1	0	-------	------	--------	0.333155
2	-0.0065	-0.0016	0.0025	0.001705	.333450
3	-.0404	-.0085	.0133	.008900	.324550
4	-.2452	-.0515	.0803	.053668	.270882
5	-.5663	-.1615	.2519	.084167	.186715
6	-1.2787	-.3583	.5589	.186715	0

TABLE V.- OUTER-SECTION STIFFNESS FACTORS

Stiffness factor	Loadings 1 and 2	Loadings 3 and 4
k_1M, lb	15892.86	0
k_2T, lb	0	-2078.91
k_3, lb/radian	-1103484	-1103484
k_4M, lb	15892.86	0
k_5V, lb/in.	-178.5714	0
k_6T, lb/in.	0	156.0246
k_7, lb/in./radian	27943	27943
k_8V, lb/in.	0	0
k_9T, lb/in.	0	50.7371
$k_{10}V$, lb/in.	-178.5714	0

TABLE VI.- STRESS DISTRIBUTION IN CARRY-THROUGH SECTION

(a) When ends are rotated by the amount $\left(\psi_1 + \psi_3 \sin \Lambda + \phi_3 \cos \Lambda\right) = 1 \times 10^{-6}$ radians

Stress	Symmetrical	Antisymmetrical
σ_8^B, psi	1.3100	0.7303
σ_{9-}^B, psi	1.3100	0.2460
σ_{9+}^B, psi	1.1882	0.2231
$\tau_{c,9}^B$, psi	0	1.6177
$\tau_{c,10}^B$, psi	0	1.6177

(b) When ends are warped by the amount $\left(\psi_1 - \psi_3 \sin \Lambda - \phi_3 \cos \Lambda\right) = 1 \times 10^{-6}$ radians

Stress	Symmetrical	Antisymmetrical
σ_8^W, psi	1.6041	1.5662
σ_{9-}^W, psi	1.2373	0.4972
σ_{9+}^W, psi	0.9705	0.3900
$\tau_{c,9}^W$, psi	-0.2361	-1.2140
$\tau_{c,10}^W$, psi	0	0.1038
$\tau_{b,9}^W$, psi	0.3683	0.2530
$\tau_{b,10}^W$, psi	0	-1.0185

TABLE VII.- CARRY-THROUGH SECTION STIFFNESS FACTORS

Stiffness factor	Loadings 1 and 3	Loadings 2 and 4
k_{11}, lb/radian	3277276	1827064
k_{12}, lb/radian	-1546392	-1509857
k_{15}, lb/radian	3277276	1827064
k_{16}, lb/radian	1546392	1509857
k_{19}, lb/in./radian	0	126178
k_{20}, lb/in./radian	18418	94691
k_{23}, lb/in./radian	0	0
k_{24}, lb/in./radian	-18418	-12651
k_{27}, lb/in./radian	0	-126178
k_{28}, lb/in./radian	18418	94691

TABLE VIII.- SYSTEM OF EQUATIONS FOR EACH LOADING CONDITION

Loading 1	Symmetrical tip bending load of 2500 lb
Loading 2	Antisymmetrical tip bending load of 2500 lb
Loading 3	Symmetrical tip torque load of 43,420 in.-lb
Loading 4	Antisymmetrical tip torque load of 43,420 in.-lb

Loading 1 Loading 2 Loading 3 Loading 4	Loadings 1 and 2 Loadings 3 and 4	Loadings 1 to 4

7.562904 7.459566 5.865823 5.762485	2.787400	-5.880185 -5.807114 -5.880185 -5.807114	3.189065 1.491984	-4.510000 -2.109975	-3.092785 -3.019714 -3.092785 -3.019714	0	ψ_1	-0.031786 0
-3.189065 -1.491984	2.787400	-5.434802	-6.933040 -5.235959	4.510000 2.109975	2.647402	0	ψ_2	0.031786 0
-0.549024 0.063013	0.260050 0.201223	0	-0.181257 0.347587	5.357149 3.705018	-1.363534 -1.304707	-3.477231 -2.690647	ψ_3	0.015893 -0.0020789
-0.016499	1.035295	0.363038	0.016499	-0.004610	0.004610	-1.375000	ϕ_1	0 -0.0000507
2.935596 2.462581	5.231885 5.114242	5.906194	1.981974 1.342586	2.556713 1.652486	0.920518 1.038161	-18.766850 -17.193682	ϕ_2	-0.005357 0.0057558
-0.117596 -0.080792 -0.117596 -0.080792	2.787400	-7.131781 -7.157806 -7.131781 -7.157806	2.517477	-1.103484	5.614173 5.588148 5.614173 5.588148	0	ϕ_3	0.015893 0.0020789
2.942805 0.943574 2.942805 0.943574	-3.487400	7.611069 6.124321 7.611069 6.124321	-0.494977	-1.803484	6.627153 5.140405 6.627153 5.140405	0	$\frac{w_2}{b}$	0.015893 0.0020789

NACA

TABLE IX.- JOINT DISPLACEMENTS FOR EACH LOADING CONDITION

Displacement	Loading 1	Loading 2	Loading 3	Loading 4
ψ_1, radians	0.0003681	0.0019304	-0.0002970	-0.0005616
ψ_2, radians	0.0029693	0.0040942	-0.0013392	-0.0015269
ψ_3, radians	0.0012872	0.0024238	-0.0006535	-0.0008414
ϕ_1, radians	0.0005019	0.0005217	-0.0003813	-0.0003817
ϕ_2, radians	0.0055292	0.0066615	-0.0012307	-0.0014186
ϕ_3, radians	0.0038611	0.0050147	0.0001279	-0.0000604
w_1/b, radians	0	0	0	0
w_2/b, radians	0.0025716	0.0037002	-0.0011405	-0.0013282
w_3/b, radians	0	0	0	0

NACA

TABLE X.- CALCULATED LOADS AND STRESSES AROUND THE TRIANGULAR SECTION OF THE SWEPT BOX BEAM FOR EACH LOADING CONDITION

Loading 1 Symmetrical tip bending load of 2500 lb.
Loading 2 Antisymmetrical tip bending load of 2500 lb.
Loading 3 Symmetrical tip torque load of 43,420 in.-lb.
Loading 4 Antisymmetrical tip torque load of 43,420 in.-lb.

	Flange								Web or cover							
	P_n (lb)				σ_n (psi)				q_n (lb/in.)				τ_n (psi)			
	Loading				Loading				Loading				Loading			
n	1	2	3	4	1	2	3	4	1	2	3	4	1	2	3	4
1	8110	8148	-1005	-1006	4406	4426	-1167	-1168	87.7	86.9	78.5	78.5	1124	1114	1007	1007
2	14052	14076	-580	-580	7634	7647	-673	-673	-132.0	-132.6	118.1	118.1	-1692	-1699	1514	1514
3	17734	17710	580	580	[a]10767	[a]10739	672	672	225.2	224.6	118.1	118.1	2887	2879	1514	1514
4	4689	4656	-1911	-1911	11675	11593	-4758	-4758	-46.6	-46.0	88.7	88.7	-932	-920	1774	1774
5	2342	2349	-1365	-1365	-----	-----	-----	-----	-110.4	-110.7	64.3	64.3	-2208	-2214	1287	1287
6	18197	18164	-2307	-2306	[a]10501	[a]10466	[a]-996	[a]-995	-60.3	592.0	1.4	-144.1	-773	7589	18	-1848
7	8077	8110	-2076	-2076	[a]2	[a]37	[a]-756	[a]-757	60.3	42.1	-1.4	-1.0	1205	843	-28	-19
8	9224	9231	1761	1761	17107	17120	3266	3266	-60.3	-1222.5	1.4	158.5	-773	-15673	18	2032
9	-5737	-5764	710	711	-10640	-10690	1317	1319	292.6	311.5	26.1	25.7	2341	2492	209	206
10	14052	14076	-580	-580	[a]6501	[a]6528	-672	-672	219.6	219.4	-39.5	-39.5	1757	1755	-316	-316

[a]Indicates a stress composed of a bending and warping component.

TABLE XI.- CALCULATED STRESS DISTRIBUTION IN THE OUTER SECTION OF THE SWEPT BOX BEAM FOR EACH LOADING CONDITION

FLANGES

n	σ_F (psi)				σ_R (psi)			
	Loading				Loading			
	1	2	3	4	1	2	3	4
6	6501	6528	-672	-672	10767	10740	672	672
5	6622	6634	-298	-298	8512	8500	298	298
4	6091	6096	-129	-129	6909	6904	129	129
3	4298	4298	-21	-21	4432	4432	21	21
2	2220	2220	-4	-4	2242	2242	4	4

WEBS

n	τ_f (psi)				τ_r (psi)			
	Loading				Loading			
	1	2	3	4	1	2	3	4
6	-1691	-1699	1513	1513	2887	2879	1513	1513
5	-2020	-2023	1411	1411	2558	2555	1411	1411
4	-2203	-2204	1352	1352	2375	2374	1352	1352
3	-2275	-2275	1329	1329	2303	2303	1329	1329
2	-2286	-2286	1327	1327	2292	2292	1327	1327

COVERS

n	τ_b (psi)			
	Loading			
	1	2	3	4
6	-932	-920	1774	1774
5	-420	-415	1935	1935
4	-134	-132	2025	2025
3	-22	-22	2061	2061
2	-4	-4	2066	2066

TABLE XII.- CALCULATED STRESS DISTRIBUTION IN THE CARRY-THROUGH SECTION OF THE SWEPT BOX BEAM FOR EACH LOADING CONDITION

FLANGES

n	σ_F (psi)				σ_R (psi)			
	Loading				Loading			
	1	2	3	4	1	2	3	4
8	2	36	-756	-757	10500	10466	-996	-995
9-	1202	112	-784	-257	9300	3424	-968	-333
9+	1587	305	-722	-238	7939	2903	-866	-298

WEBS

n	τ_f (psi)				τ_r (psi)			
	Loading				Loading			
	1	2	3	4	1	2	3	4
9	-773	7589	18	-1848	-773	-15673	18	2032
10	0	11977	0	-1948	0	-11284	0	1932

COVERS

n	τ_b (psi)			
	Loading			
	1	2	3	4
9	1205	843	-28	-19
10	0	-3391	0	77

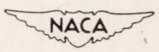

TABLE XIII.- CALCULATED DEFLECTIONS AND ROTATIONS OF THE OUTER SECTION OF THE SWEPT BOX BEAM FOR EACH LOADING CONDITION

Loading 1 Symmetrical tip bending load of 2500 lb
Loading 2 Antisymmetrical tip bending load of 2500 lb
Loading 3 Symmetrical tip torque load of 43,420 in.-lb
Loading 4 Antisymmetrical tip torque load of 43,420 in.-lb

n	x	Deflection[a] (in.)								Rotation[b] (radians)							
		Front spar				Rear spar				Perpendicular to spars				Parallel to flight direction			
		Loading				Loading				Loading				Loading			
		1	2	3	4	1	2	3	4	1	2	3	4	1	2	3	4
6	0	0.077	0.110	-0.034	-0.040	0	0	0	0	0.00257	0.00370	-0.00114	-0.00133	0	0	0	0
5	11	.153	.200	-.053	-.061	.067	.080	.006	.005	.00288	.00401	-.00198	-.00216	-------	-------	-------	-------
4	22	.252	.311	-.072	-.082	.161	.187	.014	.010	.00302	.00415	-.00287	-.00305	-------	-------	-------	-------
3	44	.507	.591	-.112	-.126	.414	.464	.029	.021	.00311	.00423	-.00471	-.00489	-.00556	-.00557	-.00206	-.00206
2	66	.818	.928	-.152	-.170	.725	.800	.045	.033	.00313	.00425	-.00657	-.00676	-.00751	-.00752	-.00336	-.00336
1	88	1.159	1.293	-.192	-.215	1.065	1.166	.061	.045	.00313	.00425	-.00844	-.00862	-.00860	-.00862	-.00468	-.00468

[a]Positive deflection is downward.

[b]Positive rotation is front spar downward.

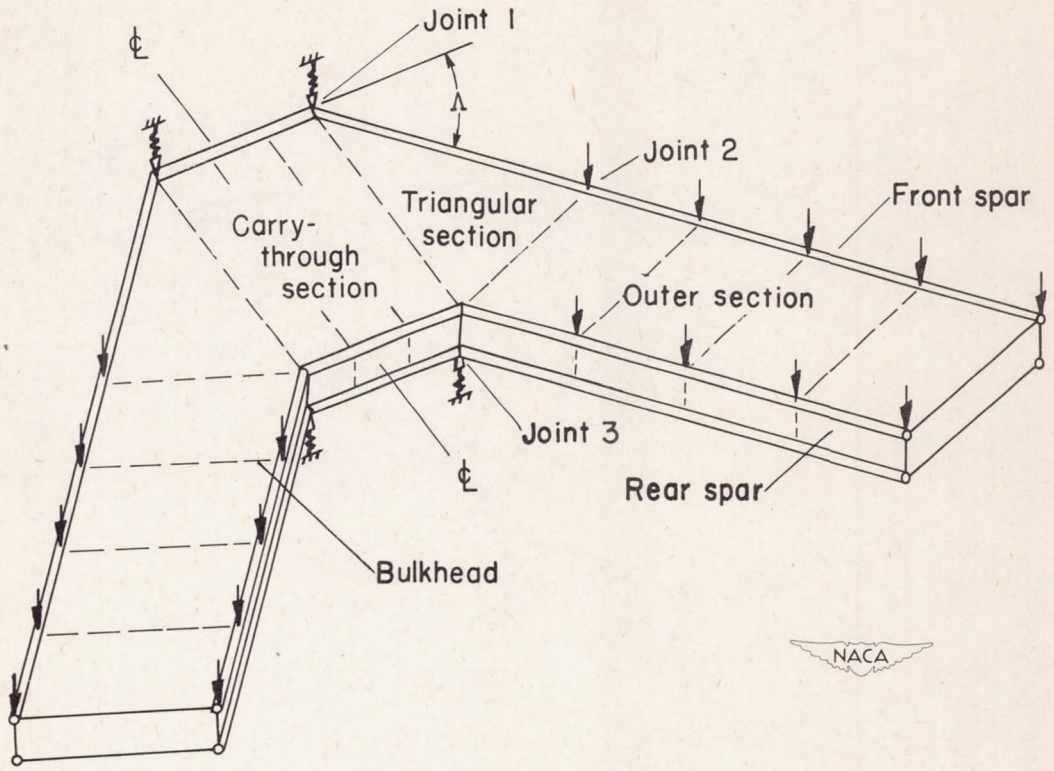

Figure 1.- Idealized sweptback box beam.

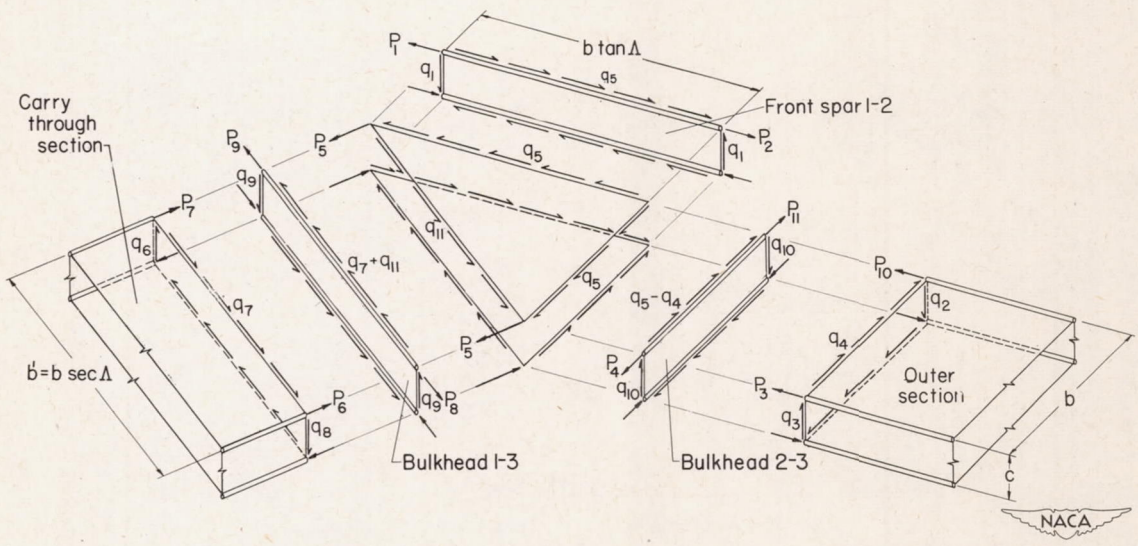

Figure 2.- Exploded view of idealized structure showing internal forces on each component around the triangular section.

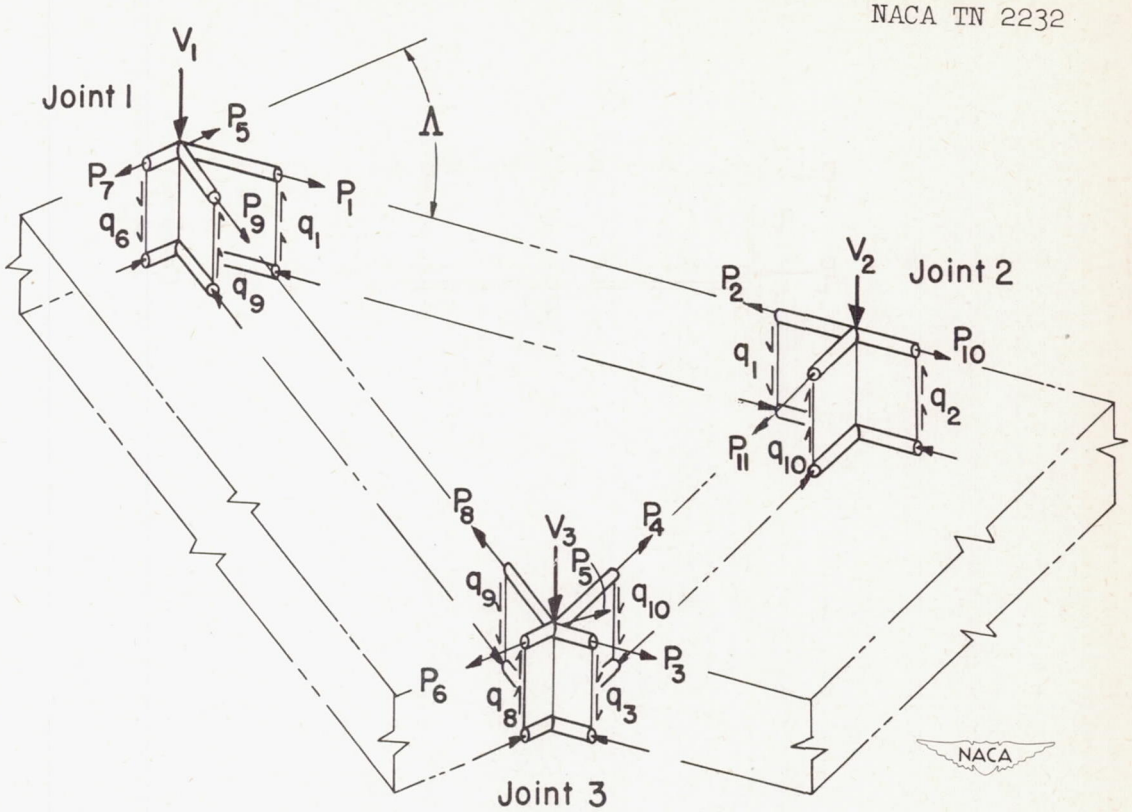

Figure 3.- Free-body diagram showing forces at the joints.

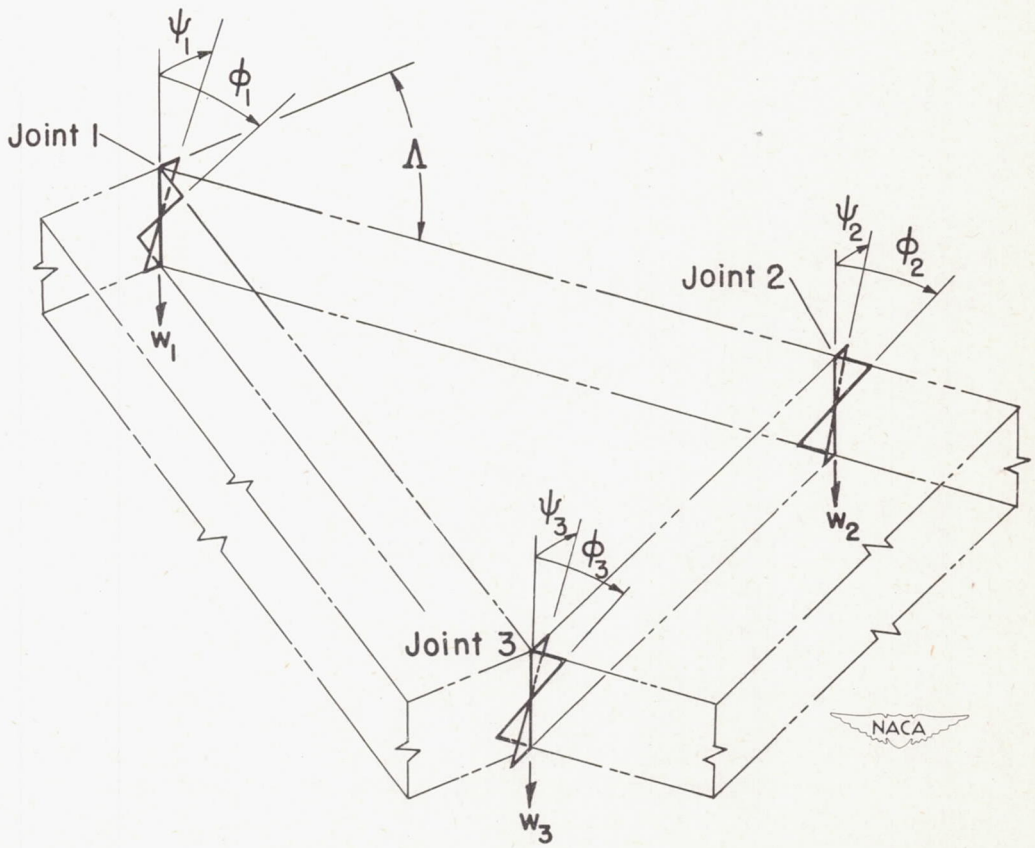

Figure 4.- Positive directions of joint displacements.

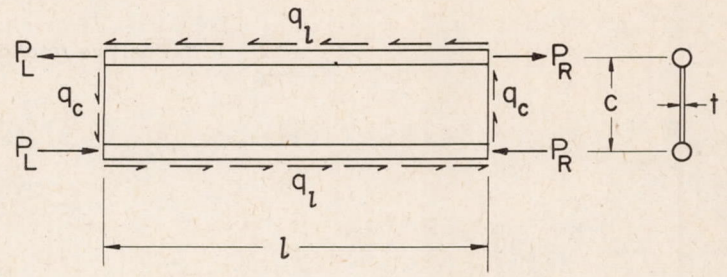

(a) Loads.

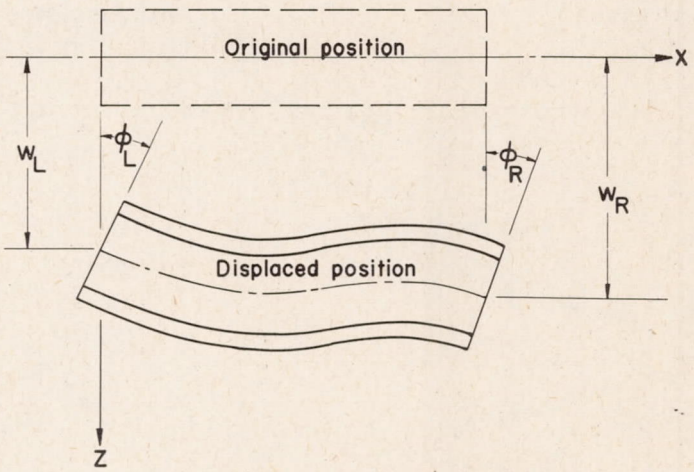

(b) Distortions.

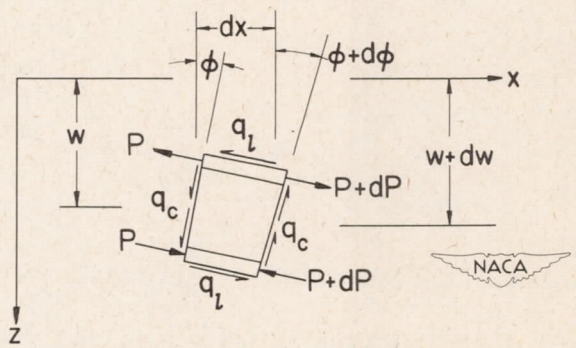

(c) Differential element.

Figure 5.- Loading and distortions of beam.

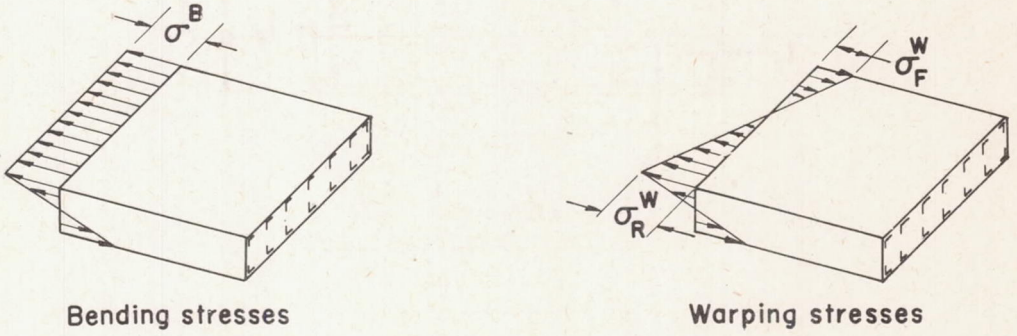

(a) Assumed stress distributions in actual structure.

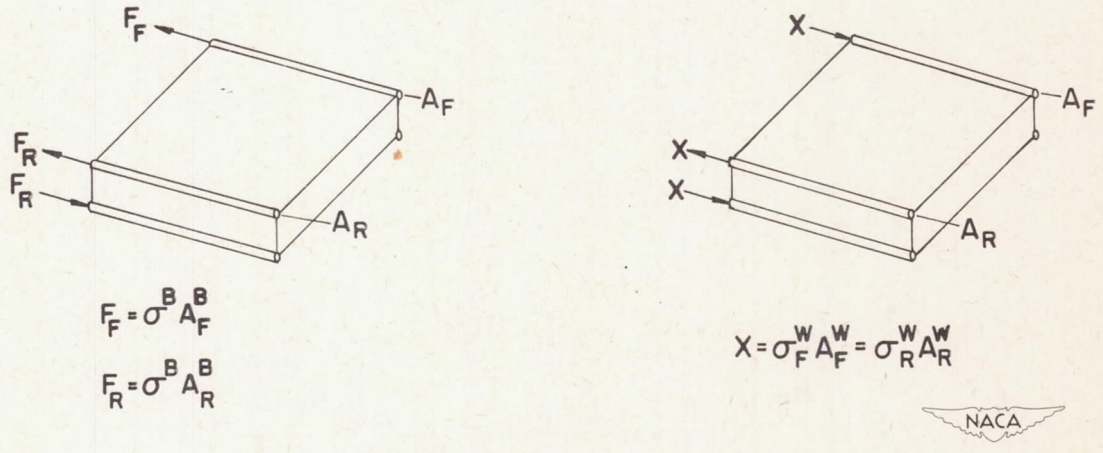

(b) Equivalent flange forces in idealized structure.

Figure 6.- Assumed distributions of stresses and forces in actual and idealized structures.

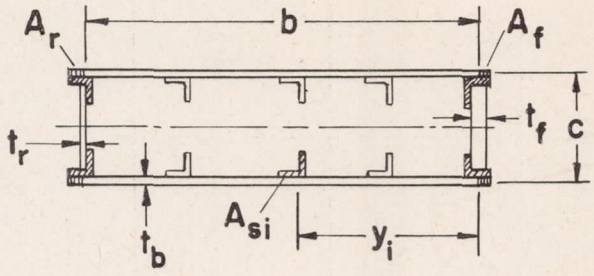

(a) Actual cross section.

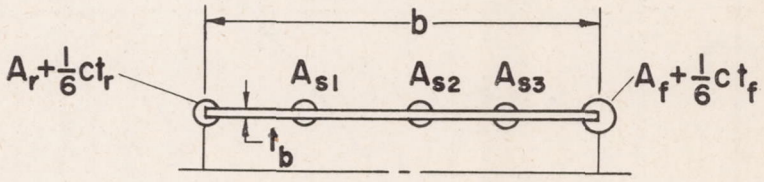

(b) Equivalent cover.

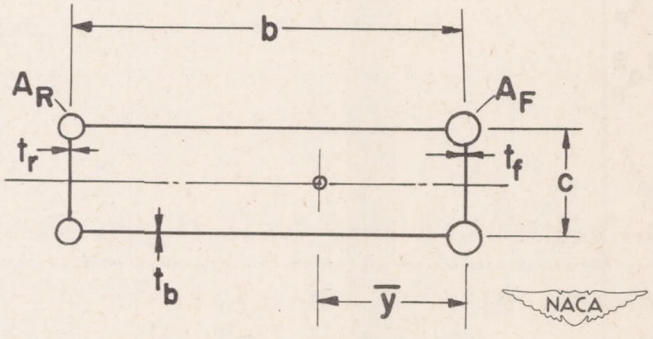

(c) Idealized cross section.

Figure 7.- Relationship between actual and idealized cross sections.

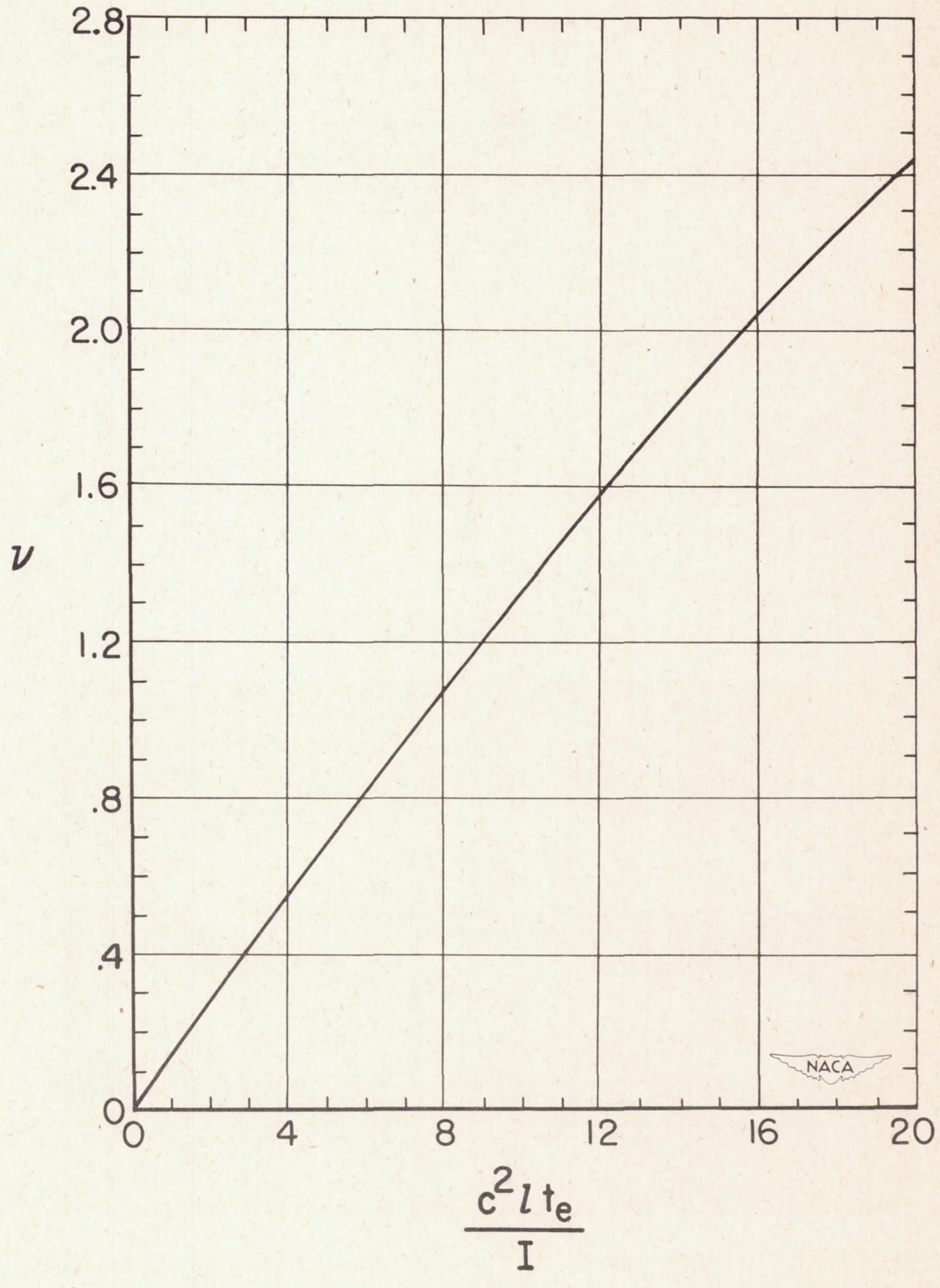

Figure 8.- Chart for determining the effective moment of inertia of bulkheads. $I_e = I(1 + \nu)$.

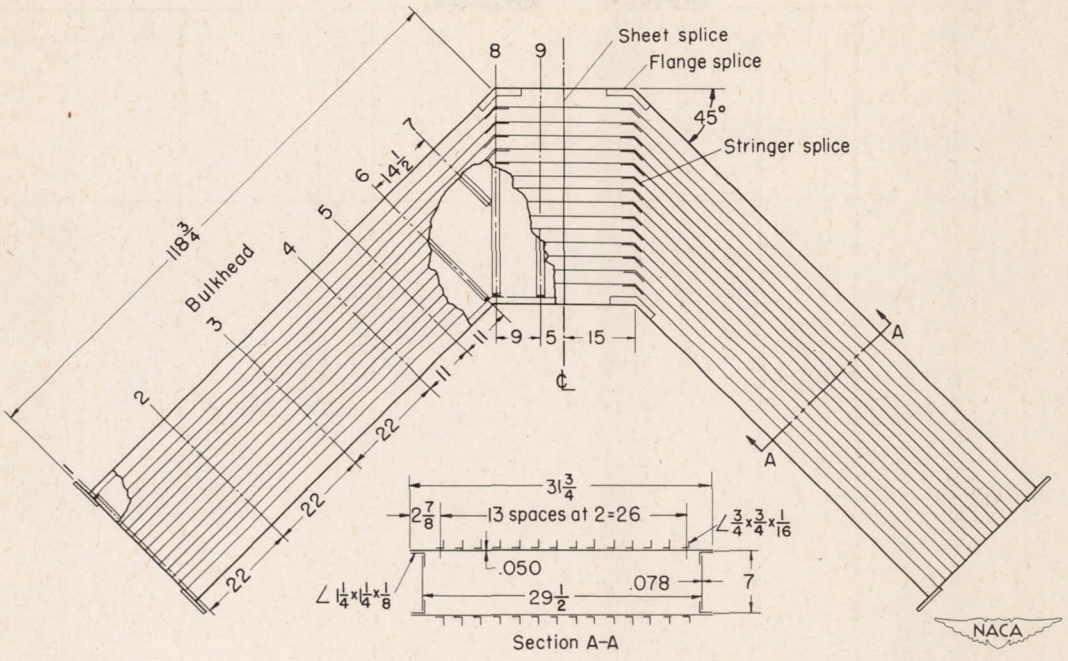

Figure 9.- Details of sweptback box beam used in tests and analyzed in illustrative example.

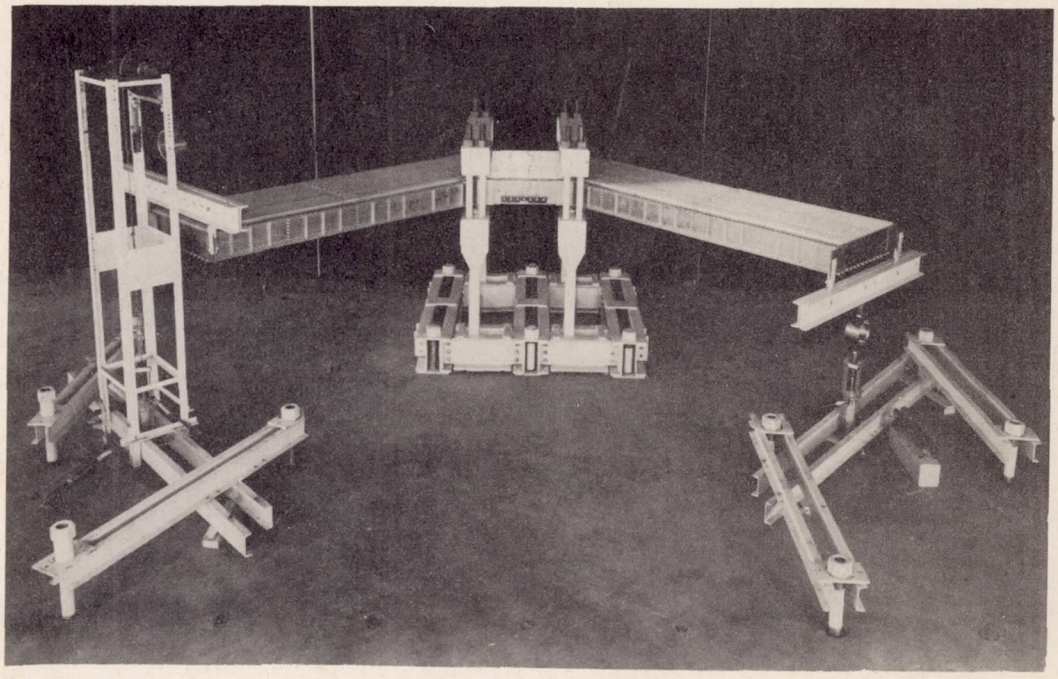

Figure 10.- Antisymmetrical bending test setup of sweptback box beam.

NACA

L-57584

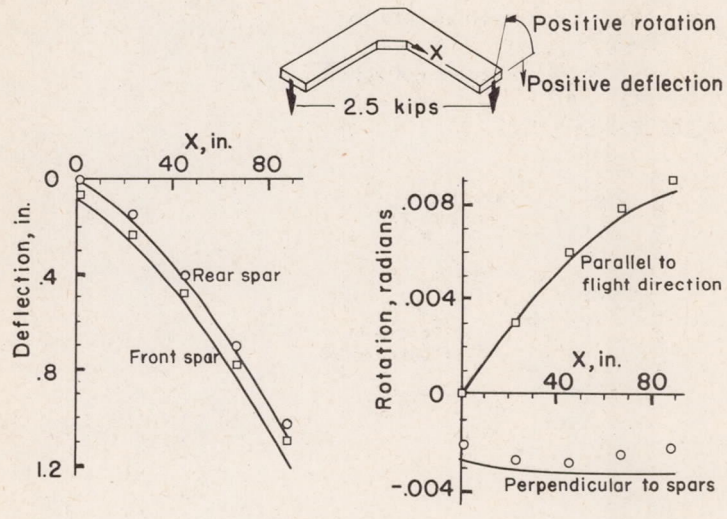

(a) Symmetrical tip bending load.

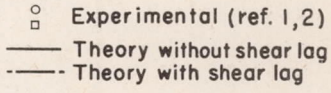

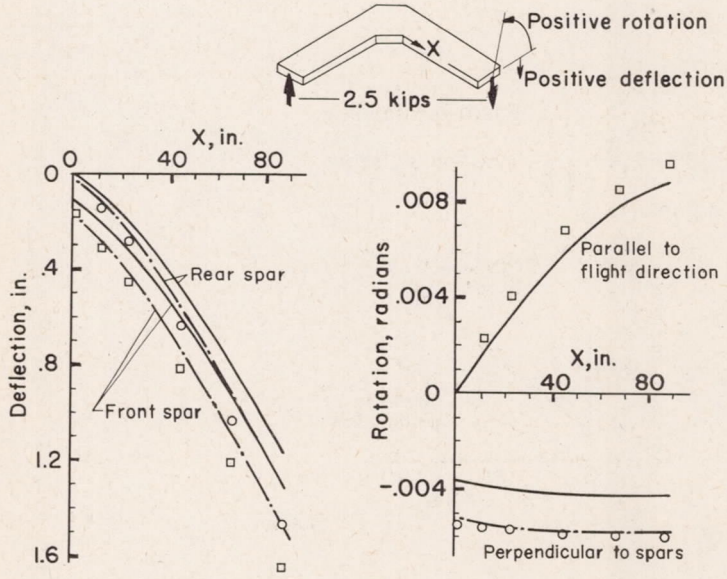

(b) Antisymmetrical tip bending load.

Figure 11.- Experimental and theoretical deflections and rotations of sweptback box beam.

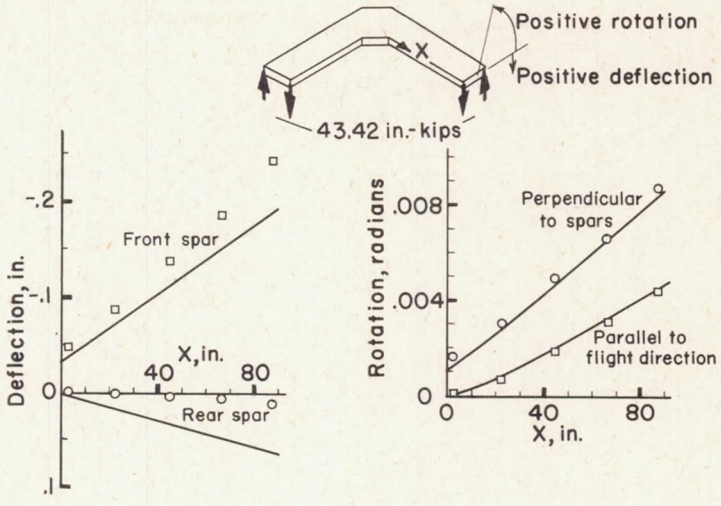

(c) Symmetrical tip torque load.

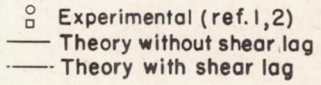

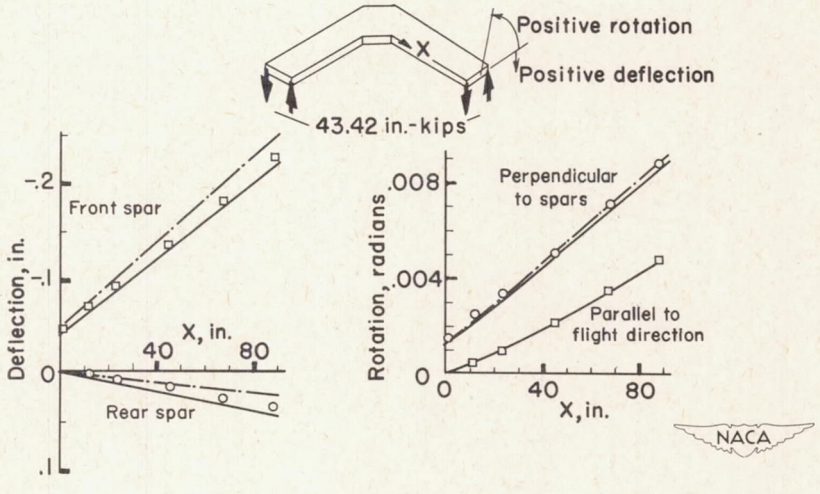

(d) Antisymmetrical tip torque load.

Figure 11.- Concluded.

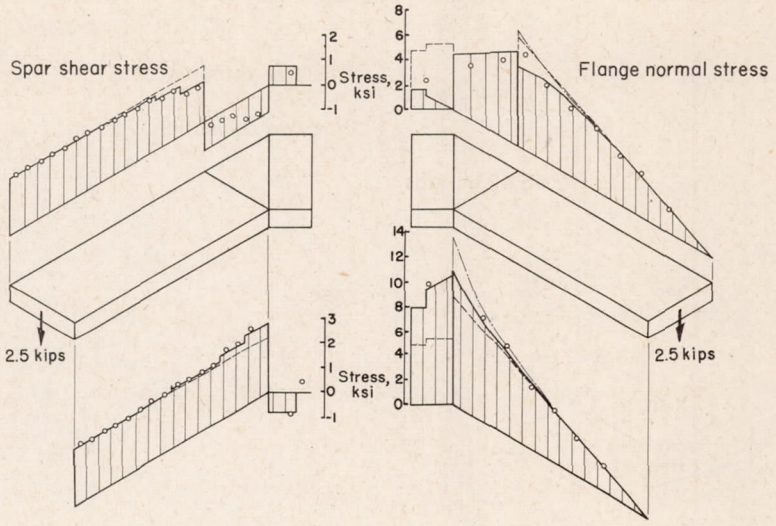

(a) Symmetrical tip bending load.

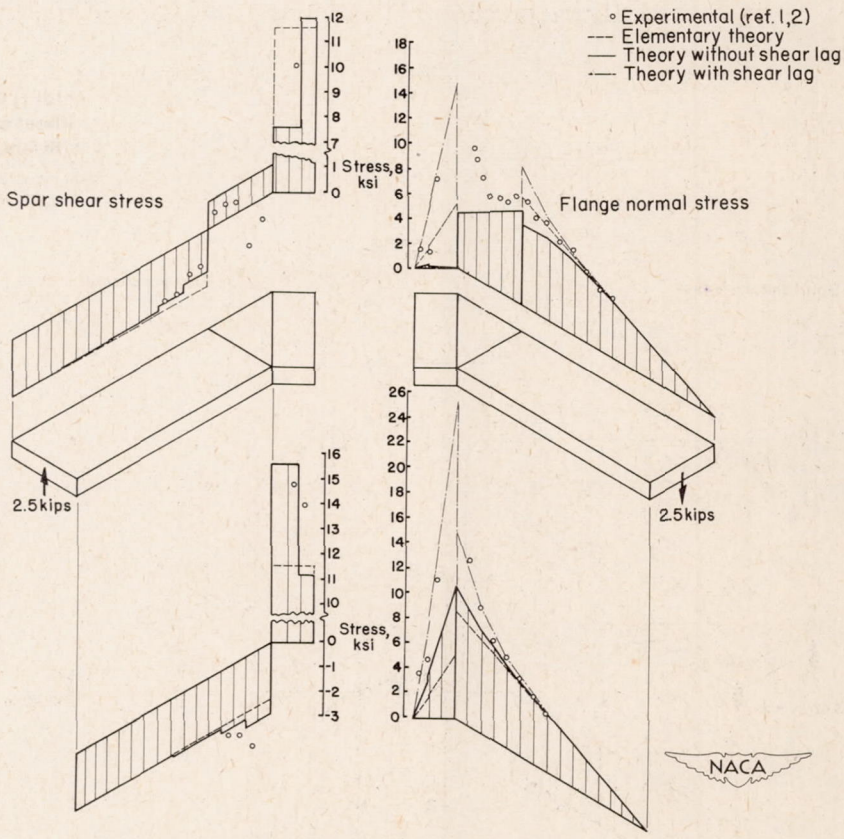

(b) Antisymmetrical tip bending load.

Figure 12.- Experimental and theoretical spanwise distribution of flange normal stresses and spar shear stresses of sweptback box beam.

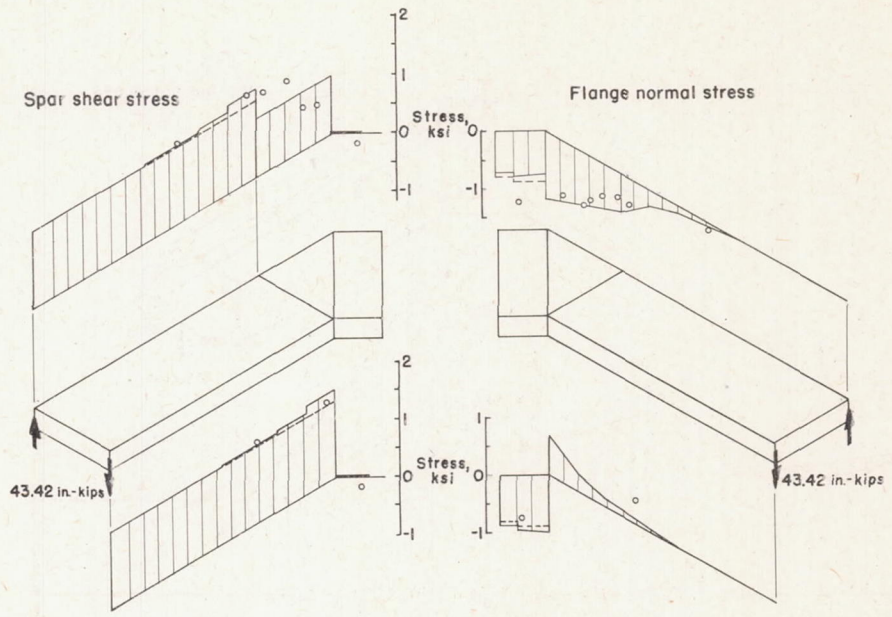

(c) Symmetrical tip torque load.

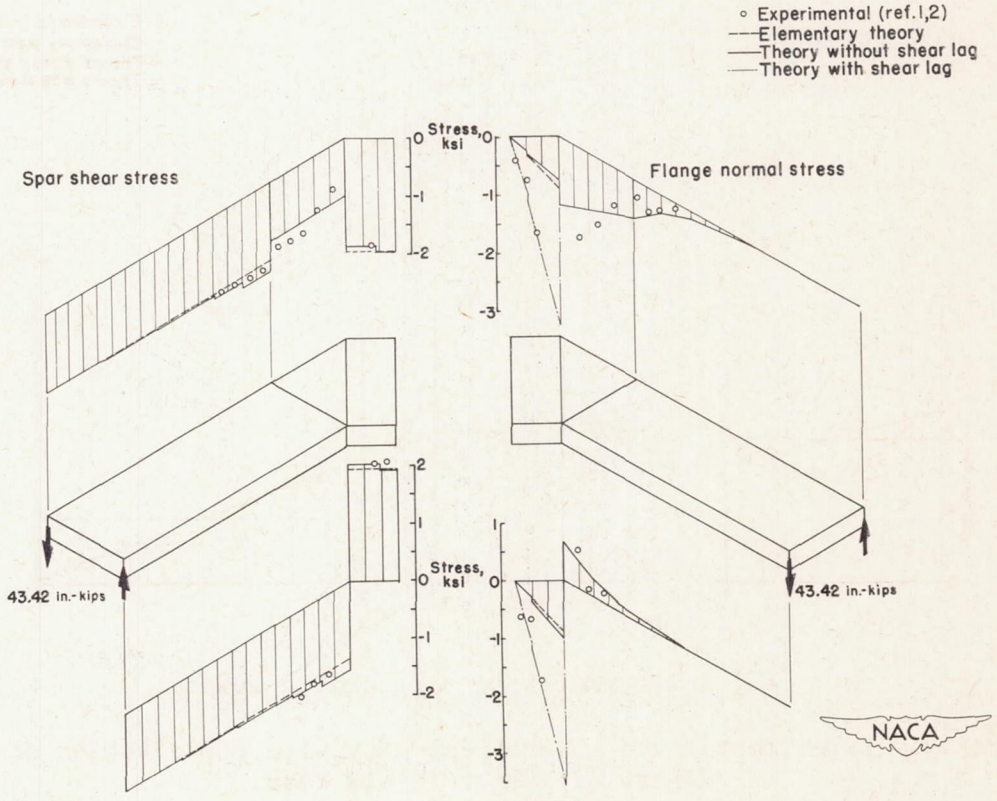

(d) Antisymmetrical tip torque load.

Figure 12.- Concluded.

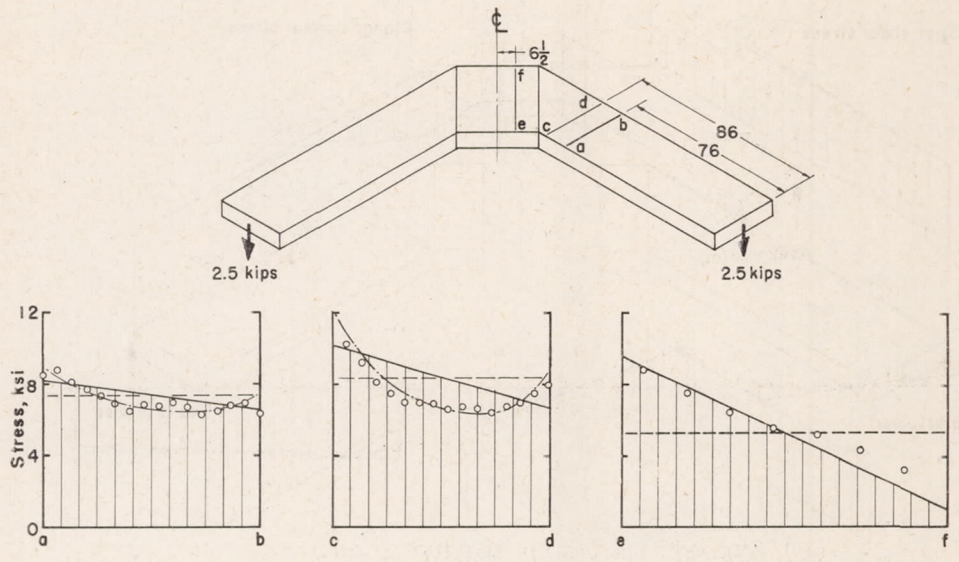

(a) Symmetrical tip bending load.

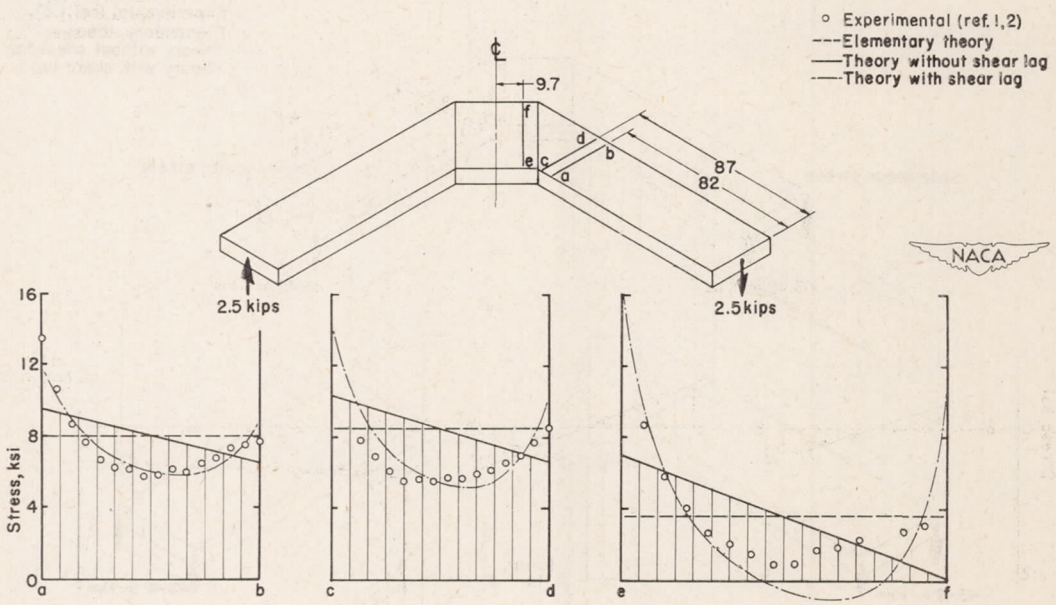

(b) Antisymmetrical tip bending load.

Figure 13.- Experimental and theoretical chordwise distribution of normal stress of sweptback box beam.

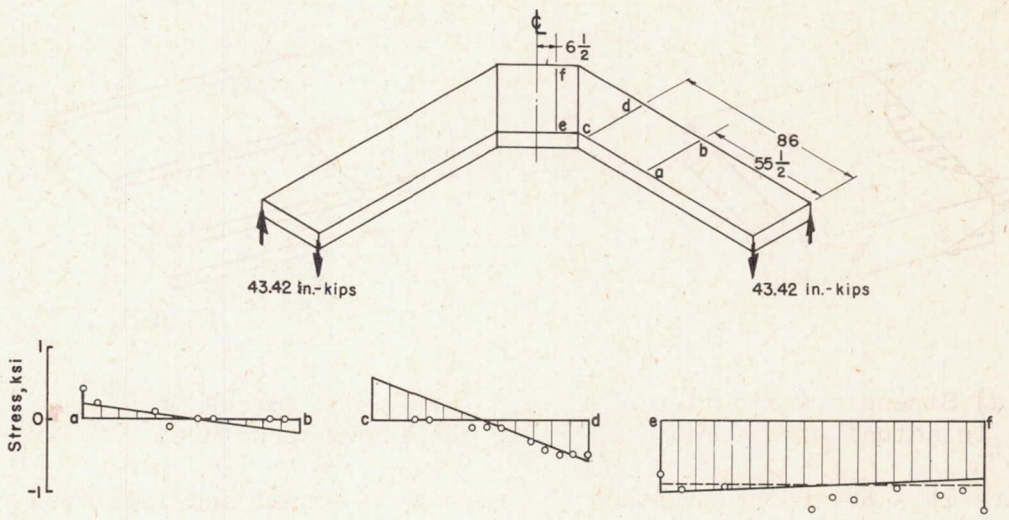

(c) Symmetrical tip torque load.

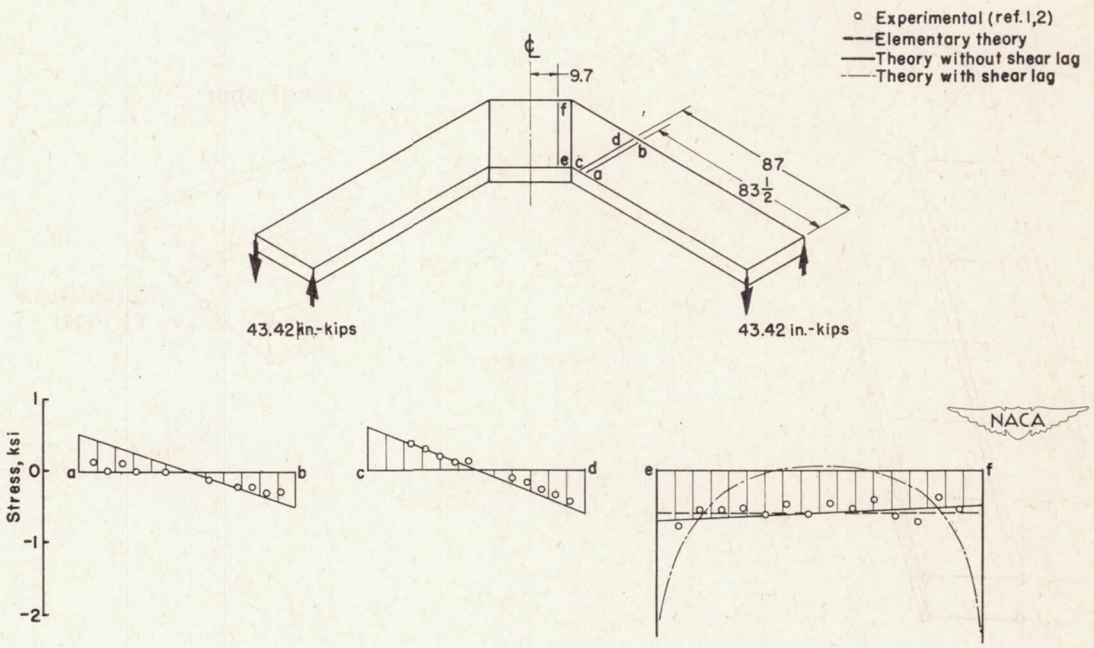

(d) Antisymmetrical tip torque load.

Figure 13.- Concluded.

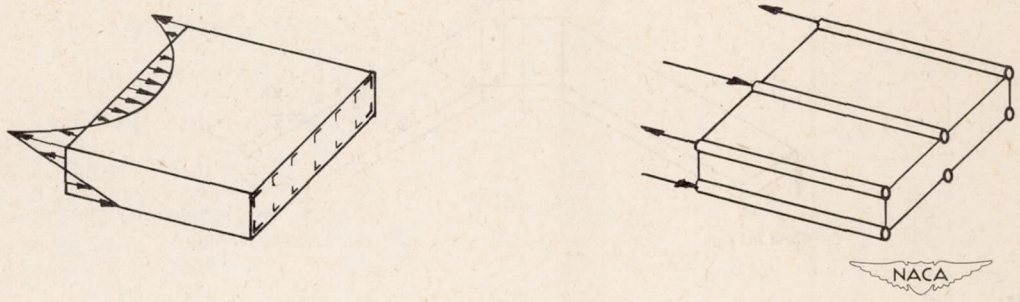

(a) Stress distribution in actual structure.

(b) Flange forces in idealized structure.

Figure 14.- Shear-lag stresses and forces in actual and idealized structures.

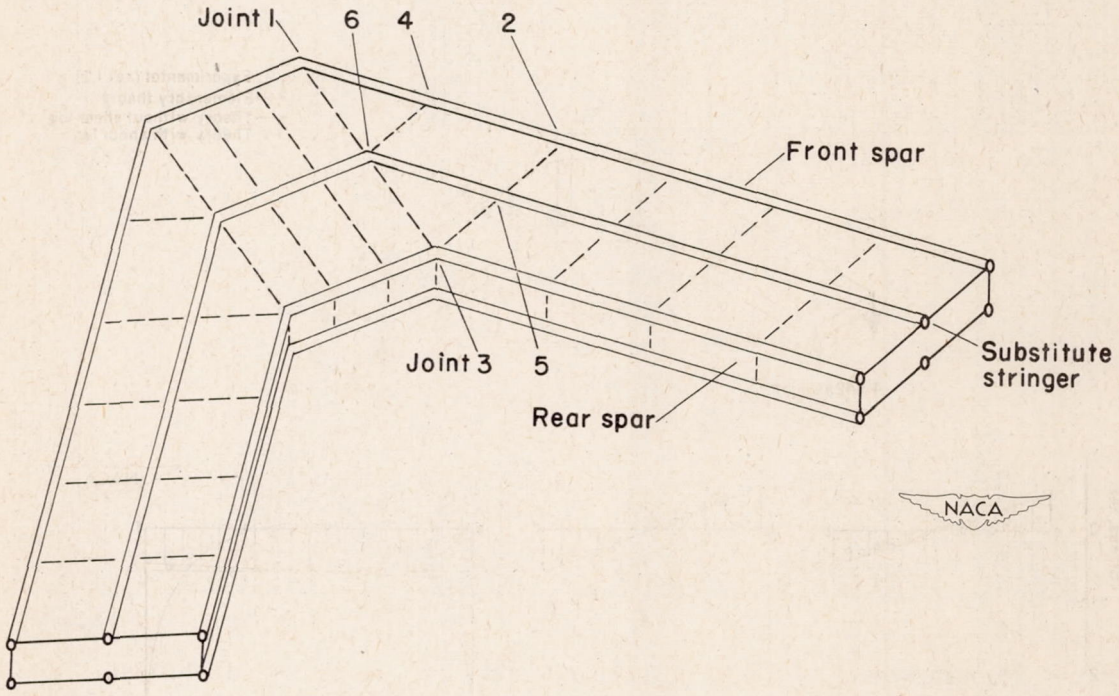

Figure 15.- Type of idealized structure required to include shear-lag effects in the analysis.

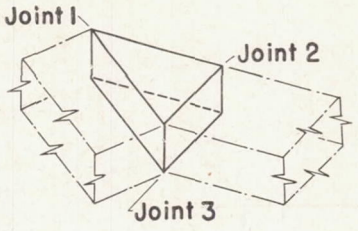

Case		Bulkhead 1-3	Bulkhead 2-3
I		Flexible	Flexible
II		Flexible	Rigid
III		Rigid	Flexible
IV		Rigid	Rigid

---- Elementary theory

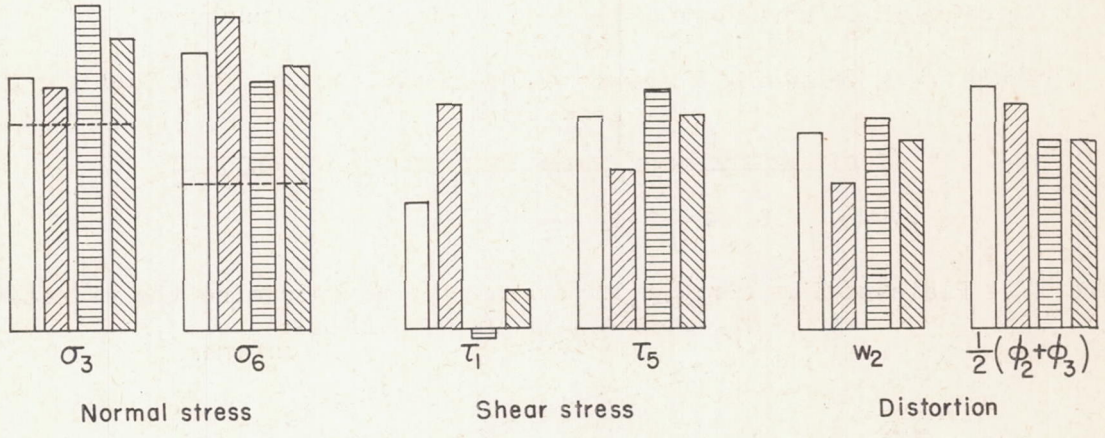

(a) Symmetrical bending.

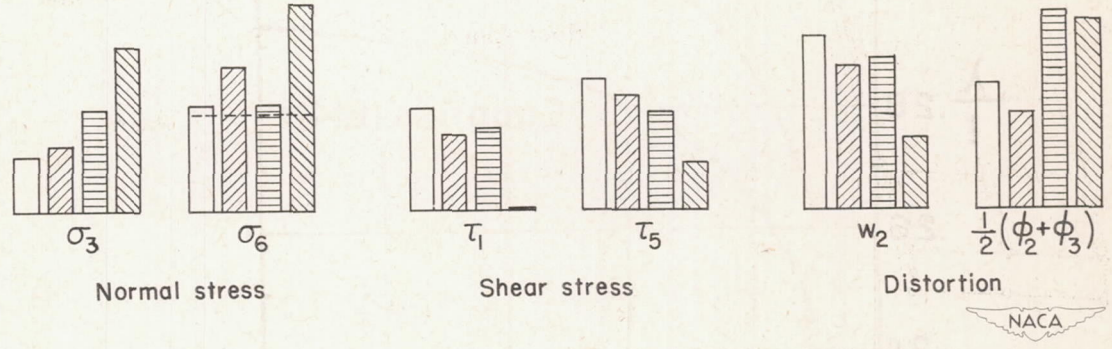

(b) Symmetrical torsion.

Figure 16.- Calculated effects of bulkhead flexibility on the stresses and distortions of a swept box beam.

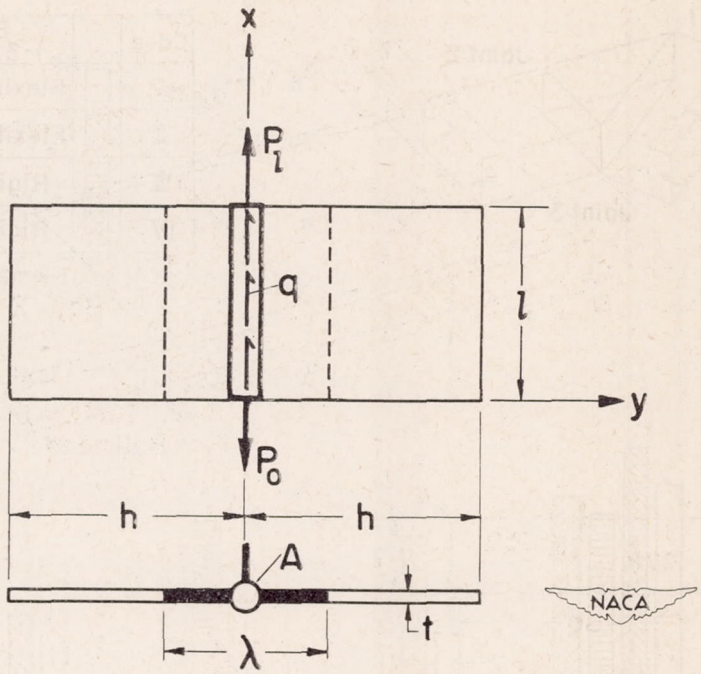

Figure 17.- Plate-stringer combination analyzed to determine the effective width of cover acting with bulkhead.

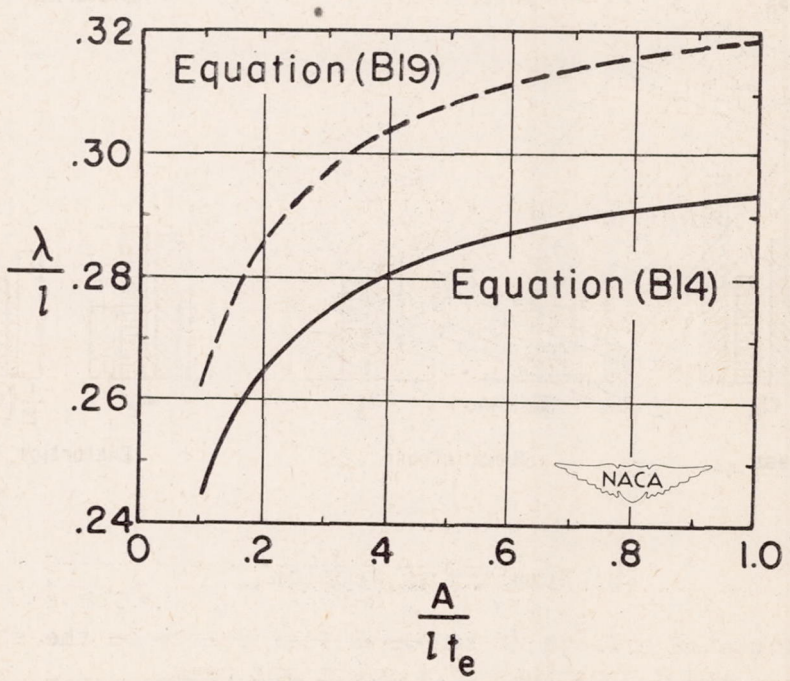

Figure 18.- Effective width of plate acting with stringer. (See appendix B).

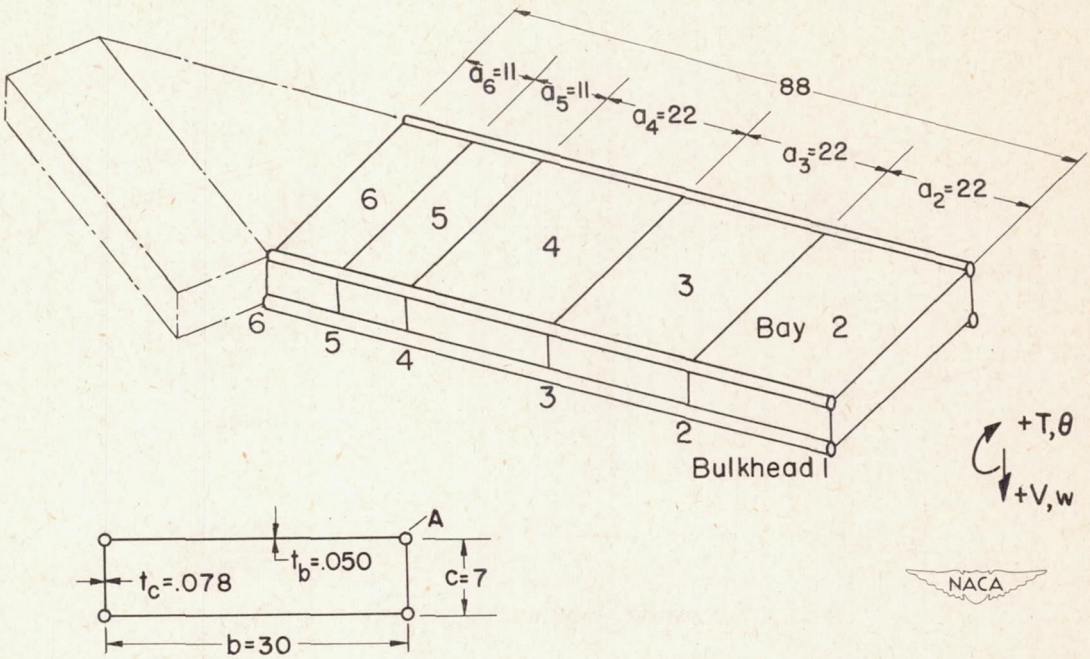

Figure 19.- Idealized outer section used in illustrative example.

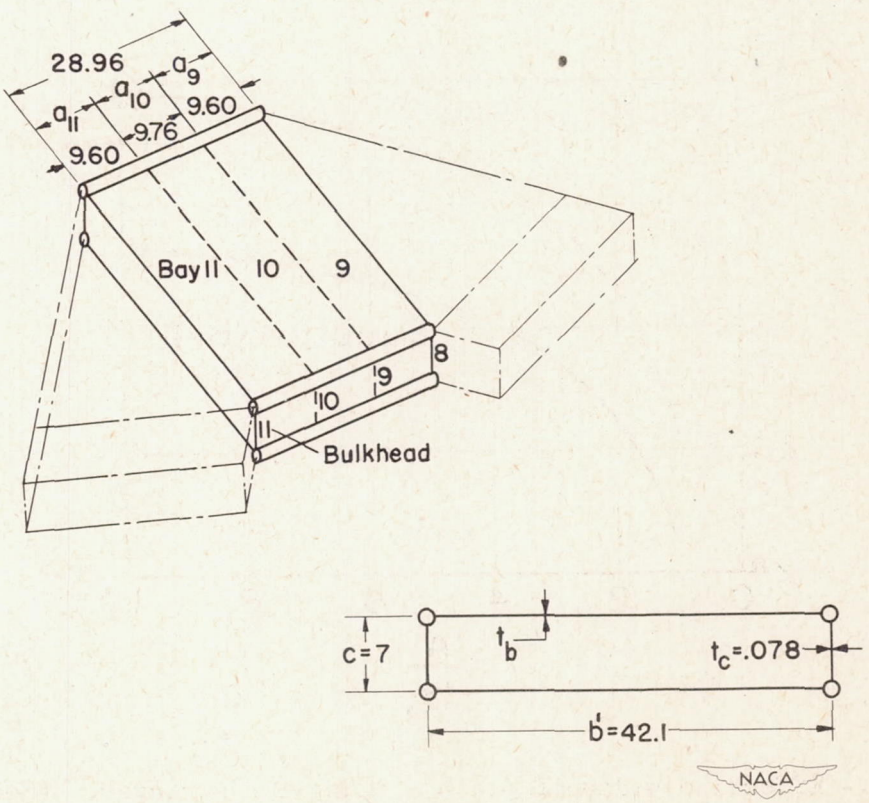

Figure 20.- Idealized carry-through section used in illustrative example.

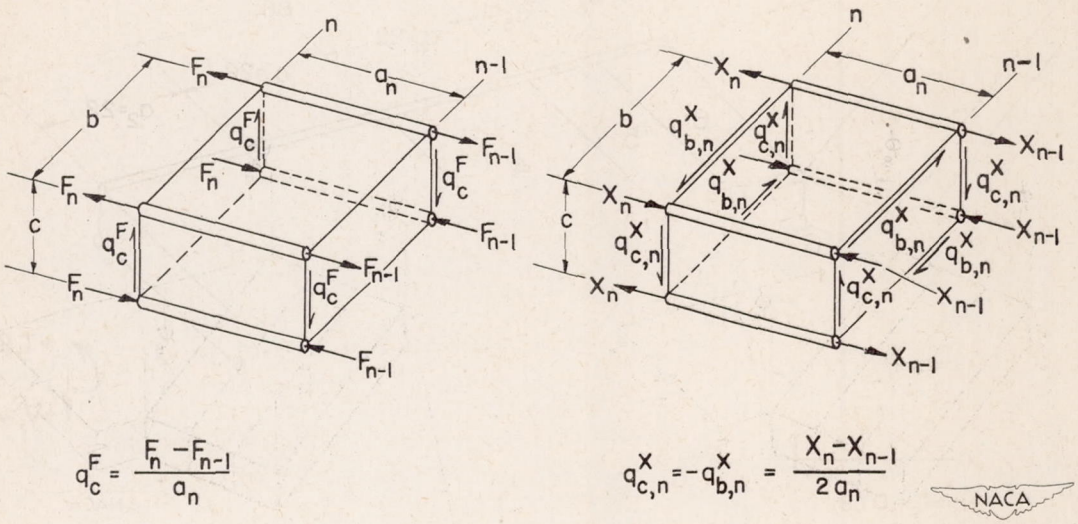

Figure 21.- Force groups of outer or carry-through sections used in illustrative example.

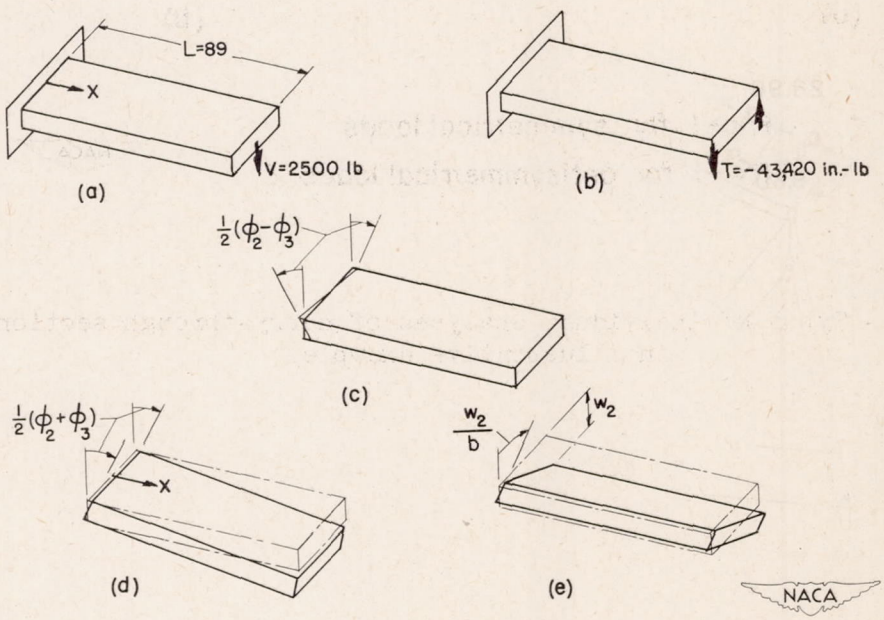

Figure 22.- Types of individual analyses of outer section used in illustrative example.

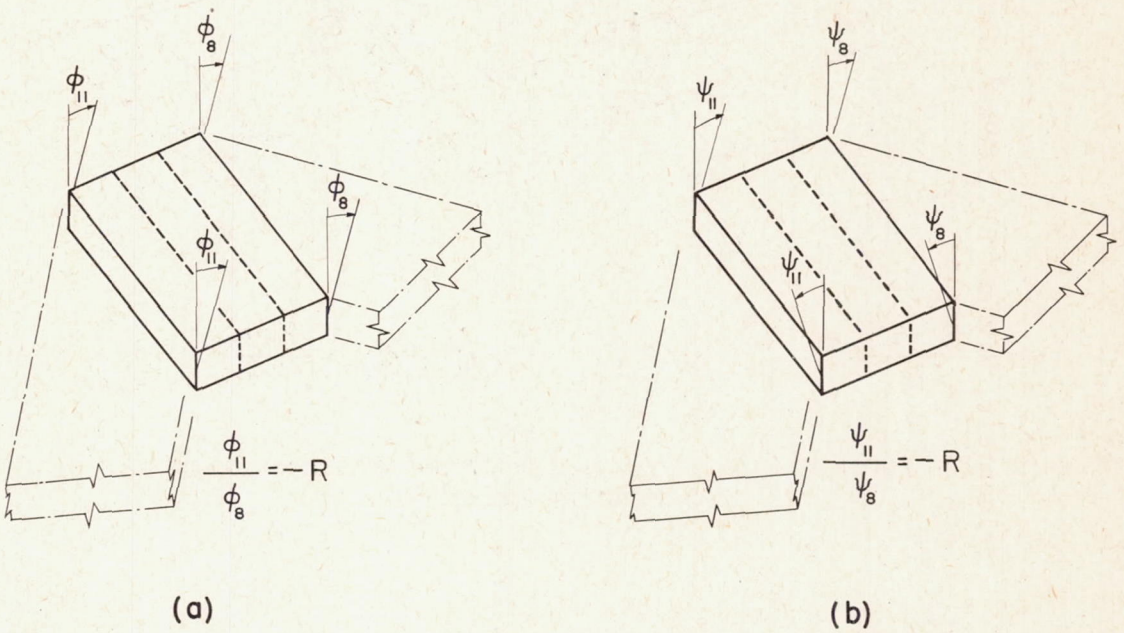

Figure 23.- Types of individual analyses of carry-through section used in illustrative example.